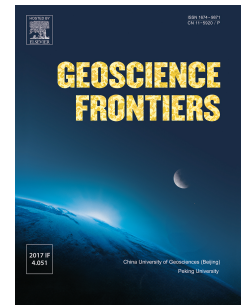


# Journal Pre-proof

New sedimentological and palynological data from the Yarkand-Fergana Basin (Kyrgyz Tian Shan): Insights on its Mesozoic paleogeographic and tectonic evolution

Julien Morin, Marc Jolivet, Dave Shaw, Sylvie Bourquin, Elena Bataleva



PII: S1674-9871(20)30112-2

DOI: <https://doi.org/10.1016/j.gsf.2020.04.010>

Reference: GSF 997

To appear in: *Geoscience Frontiers*

Received Date: 7 November 2019

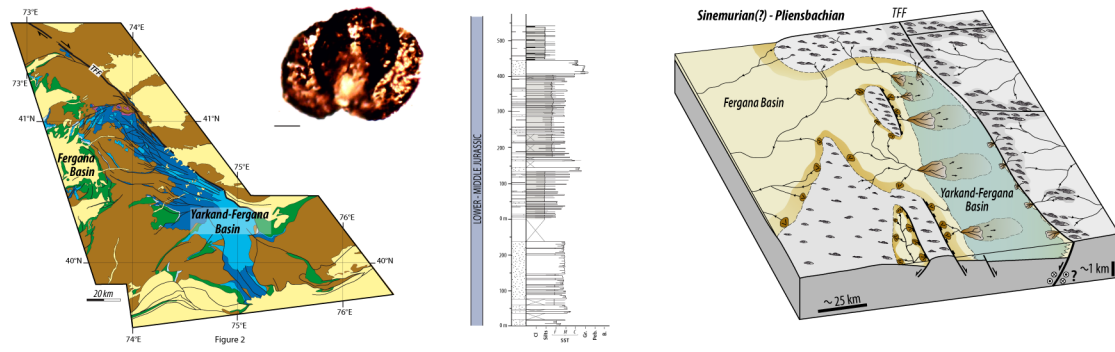
Revised Date: 4 March 2020

Accepted Date: 18 April 2020

Please cite this article as: Morin, J., Jolivet, M., Shaw, D., Bourquin, S., Bataleva, E., New sedimentological and palynological data from the Yarkand-Fergana Basin (Kyrgyz Tian Shan): Insights on its Mesozoic paleogeographic and tectonic evolution, *Geoscience Frontiers*, <https://doi.org/10.1016/j.gsf.2020.04.010>.

This is a PDF file of an article that has undergone enhancements after acceptance, such as the addition of a cover page and metadata, and formatting for readability, but it is not yet the definitive version of record. This version will undergo additional copyediting, typesetting and review before it is published in its final form, but we are providing this version to give early visibility of the article. Please note that, during the production process, errors may be discovered which could affect the content, and all legal disclaimers that apply to the journal pertain.

© 2020 China University of Geosciences (Beijing) and Peking University. Production and hosting by Elsevier B.V. All rights reserved.





# New sedimentological and palynological data from the Yarkand-Fergana Basin (Kyrgyz Tian Shan): Insights on its Mesozoic paleogeographic and tectonic evolution

Julien Morin<sup>a</sup>, Marc Jolivet<sup>a,\*</sup>, Dave Shaw<sup>b</sup>, Sylvie Bourquin<sup>a</sup>, Elena Bataleva<sup>c</sup>

<sup>a</sup> *Univ Rennes, CNRS, Géosciences Rennes, UMR 6118, CNRS – F-35000 Rennes, France*

<sup>b</sup> *Biostratigraphic Associates (UK) Ltd, 17 Woodland Avenue, Norton Green, Stoke on Trent, Staffs, ST6 8NE, UK*

<sup>c</sup> *Research Station of the Russian Academy of Sciences, Bishkek, Kyrgyzstan*

\*Corresponding author. E-mail address: marc.jolivet@univ-rennes1.fr

## Abstract

The Talas Fergana/Karatau Fault, is a major tectonic boundary separating the Kazakh-Turan domain to the west from the Tian Shan domain to the east. During the Jurassic, movements along the fault led to the opening of several basins. Still, the Mesozoic kinematics of the fault and the geodynamic mechanism that led to the opening of these basins are largely unconstrained. Located at its southwestern termination, the Yarkand-Fergana Basin is certainly the best exposed and however still poorly understood. In this study, we provide new sedimentological description of the Jurassic series from the northern part of the Yarkand-Fergana Basin as well as new palynological data. Following a Middle–Late Triassic period dominated by regional erosion, the onset of sedimentation in the Yarkand-Fergana Basin occurred during the Sinemurian(?)–Pliensbachian. The basin opened as a half graben controlled by the Talas Fergana/Karatau Fault and separated from the Fergana Basin by basement highs. Extension persisted during the late Pliensbachian–Middle Jurassic, leading to a general widening of the Yarkand-Fergana Basin. Finally, Late Jurassic–Early Cretaceous renewed tectonic activity in the area led to the inversion of the north Yarkand-Fergana Basin.

The Early to Middle Jurassic timing of development of the Yarkand-Fergana Basin suggests that the coeval movements along the Talas Fergana/Karatau Fault are not associated to the collision of the Qiangtang block along the southern margin of Eurasia. We favor the hypothesis of an opening controlled by transtension related to far field effects of back-arc extension along the Neo-Tethys subduction zone to the west.

**Keywords:** Central Asia; Talas Fergana/Karatau Fault; Extension; Jurassic

## 1. Introduction

Extending NW–SE from eastern Kazakhstan to western China (Fig. 1), the Talas Fergana/Karatau Fault is a key structural feature in Central Asia. The fault belongs to a series of parallel strike-slip lineaments that develop north and, for some of them across the Western Tian Shan range (Fig. 1). It is widely accepted that the Talas Fergana/Karatau Fault underwent multiple phases of deformation from the Neoproterozoic to the Cenozoic, especially during the Permian transpressive deformation and the late Cenozoic, ongoing orogeny (Ognev, 1939; Burtman, 1964; Allen et al., 2001; Alexeiev et al., 2009; Rolland et al., 2013). In between those two major events, during the Early-Middle Jurassic, a peculiar period of transtensional tectonics affected this structure, resulting in the formation of the South Turgay, Leontiev and Yarkand-Fergana basins (e.g. Ognev, 1946; Sobel, 1999; Allen et al., 2001; Alexeiev et al., 2017; Schnyder et al., 2017). It has been recently demonstrated that during the Jurassic, the Talas Fergana/Karatau Fault was separating a generally transpressional domain to the east from a largely extensional domain to the west (Morin et al., 2018). Nonetheless, the Mesozoic kinematics of the fault and the geodynamic mechanism that led to the opening of these basins are still poorly constrained due to the lack of detailed field data. Among the three basins, the Yarkand-Fergana is certainly the best exposed and

preserved, the South Turgay Basin being extensively covered by Cenozoic deposits while the Leontiev Basin has been strongly deformed by strike-slip movement along the Talas Fergana/Karatau Fault (e.g. Allen et al., 2001). Located in the south-western termination of the Talas Fergana/Karatau Fault, the Yarkand-Fergana Basin contains up to 5 km of Jurassic sediments in its southern part (Osmonbetov et al., 1982; Sobel, 1999). Russian geologists have provided a number of stratigraphic and structural information on the basin and its relation to the Talas-Fergana fault (e.g. Ognev, 1946; Brik, 1953; Sinitsyn, 1960; Genkina, 1977; Biske, 1982). However, its sedimentary evolution, its timing of opening and its Mesozoic kinematics remain poorly understood.

In this study, we report new sedimentological descriptions of the Jurassic series from the northern part of the Yarkand-Fergana Basin as well as new palynological data which we use to provide age constraints on those sediments. We use those data to decipher the Late Triassic to Late Jurassic–Early Cretaceous paleogeographic and tectonic evolution of the basin. The data are then discussed in terms of geodynamic implications for the kinematics of Central Asia during the Jurassic period.

## **2. Geological setting**

### **2.1. Paleozoic to Cenozoic evolution of the Talas Fergana/Karatau Fault**

The Talas Fergana/Karatau Fault is a major NW–SE oriented strike-slip structure extending for more than 2000 km from Kazakhstan to western China which has undergone multiple phases and styles of deformation during its evolution (Ognev, 1939; Sobel, 1999; Allen et al., 2001; Rolland et al., 2013; Alexeiev et al., 2009, 2017) (Fig. 1). In the Talas and Fergana ranges, the Talas-Fergana/Karatau strike-slip system initiated no earlier than the middle Permian as indicated by its crosscutting relations with Early to Middle Permian structural elements (Biske, 1982; Burtman et al., 1996; Bazhenov et al., 1999; Alexeiev et al.,

2017). In this area, the strike-slip motion is well-expressed and can reach up to 200 km of cumulated Paleozoic to Quaternary right-lateral displacement (Burtman, 1964). To the north, in the Talas and Karatau ranges, the late Paleozoic phase of deformation reactivated an older Paleozoic major structural system that corresponded to the boundary between the Karatau-Talas and Middle Tian Shan terranes (Nikolaev, 1933). This first-stage of deformation has been constrained by geochronological data from late Permian to Middle Triassic (Konopelko et al., 2013; Rolland et al., 2013; Loury et al., 2016, 2018a,b; Jourdon et al., 2017). It has been suggested that the deformation induced a maximum offset of 70 km (Alexeiev et al., 2017). The second stage of strike slip deformation, very likely related to the Early–Middle Jurassic opening of the South Turgay, Leotniev and Yarkand-Fergana basins, affected the Talas Fergana/Karatau Fault (Sobel, 1999; Moseley and Tsimmer, 2000; Allen et al., 2001; Shi et al., 2016; Alexeiev et al., 2017) although strike-slip motion has been refuted in an early study by Sinitsyn (1960). In the Kyrgyz region, a Late Triassic–Early Jurassic period of brittle reactivation of the fault has been identified by Ar-Ar dating at  $195 \pm 3$  Ma (Rolland et al., 2013). Based on a kinematic analysis of the Jurassic grabens of the southern Turgay Basin, Alexeiev et al. (2017) estimated the Jurassic right lateral maximum offset along the Talas Fergana/Karatau Fault to be up to tens of kilometers. Finally numerous observations, including seismicity point out to a third stage of strike-slip deformation along this major structure from Oligocene to present (e.g. Burtman et al., 1996; Alexeiev et al., 2017; Bande et al., 2017). In the Fergana Range, the Late Cenozoic strike slip motion is expressed by well-developed paleoseismic deformations such as fault scarps as well as displacements of the relief forms (Korjenkov et al., 2012). Moreover, several studies (e.g. Burtman, 2012; Korzhenkov et al., 2014; Feld et al., 2015; Tibaldi et al., 2015) pointed out that the TFF is still active, with an average slip rate estimated at ~9–14 mm/a based on radiocarbon and cosmogenic nuclides dating of terraces displaced by the fault (Burtman et al., 1996; Trifonov

et al., 2015; Rizza et al., 2019). However, in the Kyrgyz Tian Shan region, a significant part of the Cenozoic strike-slip displacement along the Talas Fergana/Karatau Fault is accommodated by two thrust belts (Fig. 1): (1) one that juxtaposes the Chatkal Ridge against the northern part of the Fergana Basin and (2) the other juxtaposing the Kokshaal Ridge against the western Tarim (Burtman et al., 1987; Bazhenov et al., 1993). The total amplitude of strike-slip motion during the Cenozoic is estimated at no less than 60 km, as attested by the displacement of Cretaceous facies zones in the northern parts of the Fergana and Naryn basins (Verzilin, 1968; Burtman et al., 1996).

## **2.2. Basins associated with the Talas Fergana/Karatau Fault**

### **2.2.1. The South Turgay Basin**

Located on the northern termination of the Talas Fergana/Karatau Fault, the South Turgay Basin (Fig. 1) is characterized by a series of N to NW oriented grabens and half-grabens, separated by basement highs and filled by fluvio-lacustrine sedimentary rocks (Moseley and Tsimmer, 2000; Allen et al., 2001; Shi et al., 2016; Alexeiev et al., 2017). Opening of this basin is believed to have begun during the Early Jurassic in response to renewed dextral activity along the Talas Fergana/Karatau Fault but biostratigraphic data available to support that hypothesis are limited due to the extensive Cenozoic cover that prevent access to the Mesozoic series (Moseley and Tsimmer, 2000; Allen et al., 2001; Alexeiev et al., 2017). The general evolution of this basin can be summarized as follows:

(1) An Early–Middle Jurassic rifting phase during which sedimentation consisted of coarse-grained fan delta sediments deposited along the graben margins and passing, in the central part of the basin, towards finer lacustrine deposits (Moseley and Tsimmer, 2000; Shi et al., 2016; Alexeiev et al., 2017).

(2) A period of tectonic inversion at the end of the Middle Jurassic as indicated by the presence of an angular unconformity between Middle and Upper Jurassic sedimentary rocks locally reaching 20° (Moseley and Tsimmer, 2000; Alexeiev et al., 2017).

(3) A Late Jurassic post-rift phase dominated by thermal subsidence and represented by alluvial to lacustrine sediments containing extensive coal beds (Moseley and Tsimmer, 2000; Shi et al., 2016).

Finally, nearly horizontal sequences of Cretaceous and Cenozoic sedimentary rocks unconformably overly older rocks and consist of marine and continental deposits (Alexeiev et al., 2017).

### **2.2.2. The Leontiev Basin**

The Leontiev Basin (Fig. 1) is an elongate basin containing Jurassic continental sediments and located within the central part of the Talas Fergana/Karatau Fault (Allen et al., 2001; Alexeiev et al., 2017; Schnyder et al., 2017). This basin is generally interpreted either as a pull-apart basin (Sobel, 1999) or as a dextral transtensional structure developing in a right-stepping jog in the fault system (Allen et al., 2001; Alexeiev et al., 2017). Its Jurassic sedimentary succession unconformably overlies Paleozoic basement rocks and first consists of undetermined Jurassic, pre-Toarcian conglomerates alternating with sandstones and siltstones (Buvalkin et al., 1991; Schnyder et al., 2017). In the Leontiev Basin, the Lower-Middle Jurassic deposits are tilted and are locally unconformably overlain by Upper Jurassic strata suggesting Middle–Late Jurassic tectonic deformation and tilting (Allen et al., 2001; Alexeiev et al., 2017).

### **2.2.3. The Yarkand Fergana Basin**

The Yarkand Fergana Basin is located on the south-western termination of the Talas-Fergana/Karatau fault (Figs. 1 and 2) and contains up to 5 km of Jurassic sediments in the

close vicinity of the fault and decreasing away from it (Osmonbetov et al., 1982; Sobel, 1999; Allen et al., 2001; Alexeiev et al., 2017; De Pelsmaeker et al., 2018). Most published information about the sedimentary succession and tectonic evolution of the Kyrgyz part of the Yarkand-Fergana Basin have been published in Russian (e.g. Ognev, 1946; Brick, 1953; Belgovskiy et al., 1958; Genkina, 1977). A few studies have also been done in the Chinese part of the basin. In this area, some Lower Jurassic series rest unconformably on Paleozoic basement rocks and consist of alluvial fan, fluvial and lacustrine or swamp deposits (Sobel, 1999). The lower Middle Jurassic series consist, in the close vicinity of the fault of fluvial conglomerates whereas the western part of the basin was dominated by lacustrine and swamp deposits (Sobel, 1999). The upper Middle Jurassic strata correspond to shallow lacustrine, fluvial and floodplain deposits (Sobel, 1999). Finally, the Upper Jurassic–Lower Cretaceous transition consists of up to 400 m-thick conglomeratic fluvial channel systems followed upward by Lower Cretaceous fluvial red beds deposits (Sobel, 1999). Based on these observations and on fault geometric relations, it has been proposed that the Yarkand Fergana Basin either formed as a pull-apart basin (Sobel, 1999) or as a dextral transtensional structure at a right-stepping jog in the fault system (Allen et al., 2001; Alexeiev et al., 2017). However, its timing of opening is not well constrained due to a lack of available biostratigraphic data.

### 2.3. The Fergana Basin

The Fergana Basin is situated to the west of the Yarkand-Fergan Basin (Fig. 2) which contains in its thickest part, around 10 km of Permian to Quaternary sediments. Following the late Paleozoic building of the ancestral Tian Shan, post-orogenic Upper Permian to Lower Triassic alluvial to lacustrine sediments were deposited (Clarke, 1984; Moisan et al., 2011) although the Lower Triassic series are largely unconformably resting on Paleozoic basement, suggesting ongoing tectonic movements during the Late Permian (Osmonbetov et al., 1982). The basin was then subsequently inverted, this deformation leading to a Middle–Late Triassic

erosional event (Clarke, 1984; Bande et al., 2015). Renewed subsidence started from the Early Jurassic and led to the accumulation of alluvial to lacustrine deposits during the Jurassic and Early Cretaceous (Clarke, 1984; Jolivet et al., 2017a; De Pelsmaecker et al., 2018).

### **3. Stratigraphic and tectonic framework of the Yarkand-Fergana Basin**

#### **3.1. General stratigraphy and remaining uncertainties**

The Yarkand-Fergana Basin is an elongated NW–SE orientated basin mostly filled by Jurassic clastic sediments and subdivided into three to five lithostratigraphic units depending on both the various available geological maps that diverge (Belgosvskiy et al., 1958; Luik and Zapolnov, 1960; Osmonbetov, 1980) and on the location in the basin (Figs 3 and 4). In the northern part of the basin, the Tuyuk and Chaartash (also called Uaartashskaya Fm.) formations (fms) are attributed to the Lower Jurassic and are considered to be the equivalent of the Shalitashi and Kansu fms found in the southern part of the basin (Fig. 3). In the northern part of the Yarkand-Fergana Basin, the Lower Jurassic series are followed by an undifferentiated Middle Jurassic succession. In the southern part of the basin, this unit is subdivided into the Yangye and Targa fms (Fig. 3). Finally, both the Koshbulak (north) and Kuzigongsu (south) fms are attributed to the Upper Jurassic (Fig. 3).

However, this general stratigraphic framework is not well constrained with stratigraphic ages varying from one geological map to another (Fig. 4A, B). These differences mostly concern the presence, or lack of presence, of Triassic/Lower Jurassic sediments along the western margin and in the central part of the basin but also on the occurrence, or not, of Upper Jurassic sediments in its northwestern part (Fig. 4A, B). Moreover, due to facies similarities, these different series are difficult to discriminate on the field and no available biostratigraphic data are available in this area.



Similarly, in the Fergana, South Turgay and Leontiev basins, Jurassic deposits are subdivided into several lithostratigraphic units which differ from basins to basins and are not well constrained (Fig. 3).

### **3.2. General structure and tectonic framework**

Based on geological maps (Fig. 4), the general tectonic structure of the north Yarkand-Fergana Basin is characterized by a series of faults trending parallel to and oblique to the Talas Fergana fault and by NW–SE orientated folds (Figs. 2 and 4). However, more tectonic complexities are visible in this area giving us details about the general structural pattern of the basin and clues about its evolution.

#### **3.2.1. Bayman-Bet and Kara Alma areas**

The Bayman-Bet area is located in the northwestern part of the Yarkand-Fergana Basin (Fig. 2 for location; Table 1 for GPS coordinates). In this region, an angular unconformity is observed (Fig. 5) between rather flat-lying Jurassic deposits and strongly deformed Paleozoic rocks (Osmonbetov, 1980). The base of these Jurassic deposits present fan-shaped geometries with thickening of the series toward the East (Fig. 5).

The Kara-Alma area is located in the north-west Yarkand-Fergana Basin, in the Sarik valley (Fig. 2; Table 1 for GPS coordinates). In this region, Jurassic deposits rest unconformably on strongly deformed Paleozoic rocks (Fig. 6A). The base of the series is affected by several NW–SE oriented normal faults accommodating a total offset estimated at  $\approx 100$  m (Fig. 6B).

#### **3.2.2. Chitty and Pychan areas**

The Chitty area is located in the southern part of the Yassy valley (Figs. 2 and 4). In this region, Jurassic deposits are more deformed than in the Bayman-Bet and Kara-Alma

areas. Numerous NW–SE oriented folds are visible in the field locally accommodated by E–W, south verging faults (Fig. 7A–C).

To the east, in the Pychan area, located along the Talas-Fergana/Karatau fault (Figs. 2 and 4), Jurassic sediments are also deformed and affected by thrust faults (Fig. 7D). In this location, geological maps are disagreeing (Fig. 4). Indeed, on the 1/500,000 scale map (Osmonbetov, 1980), the contact between Lower Jurassic and Paleozoic basement rocks is marked by a fault, while on the 1/200,000 scale map no fault contact is reported (Fig. 4B). The stratigraphy also varies depending on geological maps with the presence/or not of a Triassic/Lower Jurassic series. Our observations indicate, at least in the Pychan area, an absence of fault contact between the Jurassic strata and basement rocks with Jurassic sediments onlapping onto the Paleozoic carbonate units (Fig. 7E, F). Moreover, no lithological variation has been observed on the field between the supposed Triassic/Lower Jurassic series and the Lower Jurassic Chaartash Fm. It is therefore difficult to attest of the presence/or not of these two distinct units in this region without any biostratigraphic constrains.

#### 4. Sedimentological analyses and interpretations

In this study, we present new sedimentological data from the Jurassic sedimentary units of both the Yarkand-Fergana and Fergana basins (Figs. 2 and 4C; Table 1 for GPS coordinates of the different sections). Detailed sedimentological sections (1/1000), including facies and trace fossil analyses, were performed with the objective of reconstructing the evolution of the depositional environments through time. A description of the main sediment facies assemblages and their interpretation in terms of depositional environments is given in Table 2.

In the absence of available biostratigraphic or chemiostratigraphic data, we first relied on geological maps (Luik and Zapolnov, 1960; Osmonbetov, 1980) to establish the first-order

age intervals in the sediment sequences at the scale of the basin. To fully establish, and better constrain those ages, we then conducted biostratigraphical analyses from sporopollen assemblages on 22 samples collected along the Kara Alma, West Chitty and East Chitty sedimentary sections.

#### **4.1. The Yarkand-Fergana Basin**

##### **4.1.1. Bayman-Bet section**

The Bayman–Bet section (Figs. 2 and 5A; Table 1 for GPS coordinates) is limited to a ~30 m-thick outcrop of Jurassic deposits (Osmonbetov, 1980). However, the stratigraphic age of this outcrop is not well constrained with ages varying from the Lower Jurassic to the Middle-Upper Jurassic depending on geological maps (Fig. 4). The deposits consist of greyish siltstones alternating with fine to medium-grained sandstone beds locally moderately bioturbated and containing numerous plants debris. Those sediments are interpreted to be lacustrine deposits (LE2, Table 2) (Fig. 9).

Further east, and stratigraphically below the outcrop previously described, Lower-Middle Jurassic series unconformably resting on Paleozoic basement rocks are discontinuously exposed on a forested slope (Fig. 4B). Due to poor exposure, no precise sedimentological analysis has been conducted on these strata. The lower deposits consist of stacked coarse-grained sandstone beds showing faint planar cross-bedding possibly representing lacustrine delta deposits (LD, Table 2). This first sequence is overlain by alternating siltstone and sandstone layers, apparently very similar to the lacustrine facies previously described.

##### **4.1.2. Kara Alma section**

- Sedimentology:

The Kara-Alma section (Figs. 2 and 10A; Table 1 for GPS coordinates) was logged along a river incision scarp and covers ~230 m of strata attributed to the Triassic (?) and Lower Jurassic Tuyuk and Chaartash fms (Luik and Zapolnov, 1960).

At the base of the section, a ~10 m-thick succession consisting of clast-supported conglomerates with sub-angular to sub-rounded pebbles to boulders is interpreted as either alluvial fan or delta fan deposits (AF/DF, Table 2) rests unconformably on the Paleozoic basement (Fig. 10A). The next ~50 m consist of stacked medium grained sandstones alternating with siltstones containing numerous plant fragments and m-thick coal beds interpreted as lacustrine delta deposits (LD, Table 2) (Fig. 10A). These deposits are directly followed by a ~170 m-thick unit consisting of dark-grey, organic-rich siltstones and coal beds, interbedded with medium-grained sandstone beds interpreted as lacustrine deposits (LE1, LE2, Table 2) (Fig. 10A).

#### - Biostratigraphy:

Seven samples have been collected along the Kara Alma section in order to constrain the age of the deposits (Table S1; Fig. 10A for samples location). Palynomorph recovery was variably low to high and the pollen and spores are generally poorly to very poorly preserved, tending to be degraded and of dark colour (Fig. 11). However, there is enough variability in the preservation and sufficient numbers of specimens to allow for some specific identifications (See supplementary data for more details).

Samples YF-18-01 to YF-18-06 have assemblages which include *Apiculatisporites ovalis* (high abundance in sample YF-18-01), together with common *Apiculatisporites* spp., *Baculatisporites* spp., *Cyathidites* spp., *Osmundacidites* spp. and bisaccate pollen. *A. ovalis* is typical of the Early to Middle Jurassic, whilst additional *Callialasporites turbatus* (sample YF-18-04) and *Cerebropollenites thiergartii* (samples YF-18-02 and YF-18-04) provide evidence for a late-Early to Middle Jurassic age, not older than latest Pliensbachian. The

assemblage recorded from sample YF-18-07 is characterized by abundant bisaccate pollen (including *Alisporites* spp.), together with abundant *Cyathidites* spp. and *Lycopodiumsporites autroclavatidites*, and additional *Callialasporites turbatus* and *Quadraeculina anellaeformis*. This overall association of taxa suggests an age within the late-Early to Middle Jurassic, not older than latest Pliensbachian.

#### 4.1.3. Kara Tuybe section

The Kara Tuybe section (Fig. 10B) is again located in the Sarik valley, SW of the Kara Alma section (Fig. 2; Table 1 for GPS coordinates). The sedimentological section was recorded along a scarp and covers Lower-Middle Jurassic or only Middle Jurassic deposits depending on the considered geological maps (Luik and Zapolnov, 1960; Osmonbetov, 1980) (Fig. 4). The exposure is locally interrupted by large patches of vegetation.

The base of the ~220 m logged section rests unconformably on Paleozoic basement rocks and consists of a ~10 m-thick pebbly conglomerates interpreted either as alluvial or delta fan deposits (AF/DF, Table 2). The next ~5 m consist of an alternation of gravelly sandstone beds with erosional basal boundaries and normally - graded gravelly to coarse-grained sandstones interpreted as lacustrine delta deposits (LD, Table 2) (Fig. 10B). Good exposures are then lacking over a ~80 m gap in which only a few fine-grained sandstone deposits have been observed. The rest of the section consists mainly of pebbly conglomerates containing lenticular sandstone beds and of stacked beds of fine to gravelly sandstones showing 3D megaripples and occasional erosional basal boundaries. These sediments are interpreted as lacustrine delta deposits (LD, Table 2) (Fig. 10B).

#### 4.1.4. West Chitty section

Sedimentology: The West Chitty section (Fig. 12A) is located in the southern part of the Yassy valley (Fig. 2; Table 1 for GPS coordinates). This section was logged along two

distinct cliffs separated by a few hundred meters across a small river and covering Lower Jurassic to Middle Jurassic deposits based on the geological map (Osmonbetov, 1980; Luik and Zapolnov, 1960).

In this area, the 1/500,000 geological map (Osmonbetov, 1980, 1982) indicates a Late Triassic–Lower Jurassic age for the Tuyuk Fm that rests unconformably on the Paleozoic basement, although this base is not visible in the investigated sections. The Late Triassic age for the base of the series has been challenged by Genkina (1977) based on paleobotanic data. The lower part of the first section consists of a ~210 m-thick succession of heterolithic facies deposits composed of medium-grained sandstones, locally bioturbated, alternating with fine-grained sandstone beds (Fig. 12A). This succession is interpreted as deposited in a lacustrine environment dominated by turbiditic sand deposits (LE1, Table 2).

Following a tectonically deformed area consisting mainly of a fault propagated fold developing on a south-directed thrust, the first ~140 m of the second section consists of an alternation of organic-rich siltstones and fine-grained sandstones, locally bioturbated and showing occasional oscillatory ripples (Fig. 12A). The next ~260 m consists of pluri-m thick thin-bedded heterolithic facies deposits composed of organic-rich siltstones and fine-grained sandstones containing numerous plant-fragments alternating with m- to pluri-m thick medium-grained sandstone beds (Fig. 12A). Altogether, these facies associations are interpreted as lacustrine deposits (LE2, Table 2). The next ~40 m-thick units consist of stacked gravelly to coarse-grained sandstone beds interpreted as lacustrine delta deposits (LD, Table 2) (Fig. 12A). Finally, the top 80 m are dominated by organic-rich siltstone deposits interpreted as deposited in a more distal lacustrine environment (LE3, Table 2).

Biostratigraphy: Five samples were collected from the West Chitty section and analyzed in order to constrain the stratigraphic age (Table S2; Fig. 12A for samples locations). In these samples, palynomorph recovery was variably low to high with pollen and spores generally

poorly to very poorly preserved, tending to be degraded (Fig. 11) (See supplementary data for more details).

The assemblages recorded from samples Db-1 to Db-3 are of low abundance, and mainly comprise low numbers of *Cyathidites* spp., bisaccate pollen, and unidentifiable trilete spores and miospores. Occasional specimens of *Apiculatisporites ovalis* suggest an age not older than Early Jurassic (Table S2). Sample Db-4 yielded a high abundance assemblage which is dominated by trilete spores, mainly abundant *Cyathidites* spp., with additional *Concavisporites* spp., *Concavissimisporites* spp. and *Granulatisporites* spp., and a large proportion of unidentifiable trilete spores and miospores. Rare specimens of *Apiculatisporites ovalis*, *Cerebropollenites mesozoicus*, *Cerebropollenites thiergartii*, *Eucommiidites granulosus*, *Nevesisporites vallatus*, *Quadraeculina anellaeformis* and *Echinitosporites* sp. A (Bujak and Williams, 1977) suggest an Early Jurassic age, within the Pliensbachian–Sinemurian (Table S2). However, these assemblages are not well constrained. In addition possible reworking of Triassic assemblages has been identified within samples Db-2, Db-3 and Db-4 with the presence of *Aratrisporites* spp. (sample Db-4), with rare *Lunatisporites* sp. (sample Db-3) and a (?)striate bisaccate pollen (sample Db-2). This last result seems in agreement with the Early Jurassic age proposed by Genkina (1977) for the base of the series although indicating that some Triassic deposits did occur in that area that were reworked by the Lower Jurassic sediments.

#### 4.1.5. East Chitty section

Sedimentology: The East Chitty section (Fig. 12B) is located ~ 5 km eastward of the previously described West Chitty section (Fig. 2; Table. 1 for GPS coordinates). This section was recorded along a cliff covering ~ 470 m of the Lower Jurassic Chaartash Fm (Luik and Zapolnov, 1960).

The base of the logged section consists of a ~ 50 m-thick alternation of siltstone and fine-grained sandstones interpreted as lacustrine deposits (LE2, Table 2). Following a ~ 20 m-thick gap in observation, the next 360 m of the section consist mainly of siltstones and fine to medium-grained sandstones containing numerous coal beds (Fig. 11B) interpreted as deposited in variable lacustrine environments (LE1 - LE2, Table 2). The next ~ 20 m-thick consist of coarse-grained sandstones containing plant fragments and showing sigmoidal bedding (Fig. 12B), and are interpreted as lacustrine delta deposits (LD, Table 2). Finally, the top of the section is dominated by organic-rich siltstone deposits locally associated to coal beds typical of a lacustrine environment (LE2, Table 2). This last sedimentary succession extends above the section for several 10s of meters but was no logged in details.

Biostratigraphy: In the East Chitty section, 10 biostratigraphic samples were analyzed in order to constrain the covered stratigraphic interval (Table S3; Fig. 12B for samples location). In these samples, palynomorph recovery was variably low to high with pollen and spores generally poorly to very poorly preserved (Fig. 11) (See supplementary data for more details).

The assemblages are dominated by bisaccate pollen (including *Alisporites* spp.), together with the spore *Cyathidites* spp., associated with generally common *Apiculatisporites* spp., *Baculatisporites* spp. and *Osmundacidites* spp., and a large proportion of unidentifiable trilete spores and miospores (Table. S3). Rare specimens of *Callialasporites turbatus* recorded from samples D-8, D-36, D-40 and D-52, together with *Callialasporites dampieri* recorded from sample D-36, provides positive evidence for an age not older than latest Pliensbachian. Moreover, additional rare *Cerebropollenites thiergartii* (sample D-60), *Concentrisporites* sp. (samples D-8, D-16 and D-56), *Quadraeculina anellaeformis* (samples D-40 and D-76), and *Nevesisporites vallatus* (samples D-16, D-20 and D-36), and rare to common *Apiculatisporites ovalis* (samples D-8, D-16, D-36, D-60 and D-76) provide supporting evidence for an age within the late Early–Middle Jurassic (Table S3).



#### 4.1.6. Pychan section

The Pychan section (Fig. 13) is located along the Talas-Fergana fault on the eastern margin of the basin, nearby the Pychan River (Fig. 2; Table 1 for GPS coordinates). Due to its extremely remote and very high altitude position that section was not logged in details except for characteristic features.

The Lower Jurassic strata (Osmonbetov, 1980) consist of heterolithic facies composed of organic-rich siltstones and fine-grained sandstones, alternating with pluri-m-thick, normally graded, gravelly to fine-grained sandstones presenting convex-up geometries. The whole section is interpreted as deposited in lacustrine environments including fan/lobe systems (LE2, Table 2) (Fig. 13). In addition, the general geometry of these deposits indicates sedimentary input coming from the west and onlapping toward the east on Paleozoic basement rocks (Fig. 13).

#### 4.1.7. Terek section

The Terek section (Fig. 14) is located nearby the city of Terek, in the southern reach of the Kyrgyz Yarkand-Fergana Basin (Fig. 2; Table 1 for GPS coordinates) and covers up to 1400 m of Jurassic strata (Belgovskiy et al., 1958).

The first ~ 25 m-thick of the section either corresponds to alluvial fan or delta fan (AF/DF, Table 2). It is followed by an ~ 75 m-thick succession interpreted as lacustrine delta evolving toward a 320 m-thick unit corresponding to lacustrine environment dominated by turbiditic sand deposits (LE1, Table 2). The next ~ 130 m are interpreted as lacustrine delta deposits (LD, Table 2) and are followed by a ~ 700 m-thick series evolving toward more distal lacustrine environments (LE2-LE3, Table 2). Finally, this fine-grained unit is followed by sandstones and conglomerates corresponding to alluvial fan systems (AF, Table 2) (Fig. 14).

## **4.2. The Fergana Basin**

### **4.2.1. Yassy section**

The Yassy section (Fig. 15) is located in the east Fergana Basin along the Yassy river (Fig. 2) and presents ~220 m of deposits ranging from Middle Jurassic to Late Jurassic–Early Cretaceous based on geological maps (Luik and Zapolnov, 1960; Osmonbetov, 1980).

In this area, the Middle Jurassic sediments rest unconformably on Paleozoic basement rocks. The first ~ 60 m consists of yellowish, stacked medium to coarse-grained sandstones interpreted as lacustrine delta deposit (LD, Table 2) (Fig. 15). It is followed by a ~220 m thick unit of massive, reddish siltstone deposits alternating with fine to medium-grained sandstones, often bioturbated, interpreted as distal lacustrine environment deposits (LE3, Table 2) (Fig. 15). The transition between the Jurassic and the Cretaceous (Osmonbetov, 1980) is sharp, with depositional environments switching from distal lake to alluvial fan systems characterized by matrix to clast-supported conglomerates (Fig. 15). No angular unconformity is observed between the conglomerates and the underlying deposits. Pebbles are mainly composed of Paleozoic basement rocks (including cherts and metamorphic carbonates) with a few fragments of probably Mesozoic sandstones. This is consistent with the observations of Poyarkova (1969) in the eastern Fergana Basin and that of De Pelsmaecker et al. (2018) in the Tash Komyr section (NE-Fergana Basin).

## **5. Tectono-stratigraphic evolution of the north Yarkand-Fergana region**

### **5. 1. Middle–Late Triassic**

In both the north Fergana and Yarkand-Fergana basins, the Middle–Late Triassic period is generally associated to a hiatus in sedimentation (Clarke, 1988; Bande et al., 2017b) as well as by exhumation within the Kyrgyz Tian Shan (De Grave et al., 2011, 2013; Glorie et al., 2011). Altogether, these data suggest that this region was under erosion during the

Middle–Late Triassic. However, the presence, in the Bayman-Bet area (see Table 1 for location), of Lower Jurassic deposits resting unconformably above a relatively flat Paleozoic surface imply that no high relief existed in this region at that time. Middle–Late Triassic tectonic activity has been reported along the Talas Fergana/Karatau and more specifically in the Karatau Range where the time of deformation was constrained from late Permian to Triassic (Konopelko et al., 2013). In the Fergana region, Late Triassic brittle reactivation of the Talas Fault has also been described (Rolland et al., 2013). However, the impact of this Triassic tectonic activity on relief building or on the potential development of sedimentary basins in the Yarkand-Fergana region is unknown. In the Yarkand-Fergana Basin, Triassic flora has been reworked within Lower Jurassic sediments (Tables S2, S3), supporting the idea that Triassic strata are not preserved (Genkina, 1977), while restricted areas of continental sedimentation have been reported in the southwestern part of the Fergana Basin (Moisan et al., 2011). Based on all these observations, we propose that the north Yarkand-Fergana region was mainly dominated by low-reliefs with only restricted areas of sedimentation and limited tectonic activity occurring along the Talas Fergana fault (Fig. 16A).

## **5. 2. Early Jurassic: Sinemurian(?)–Pliansbachian**

The Early Jurassic corresponds to the onset of sedimentation within the North East Fergana and northern Yarkand-Fergana basins (Fig. 16B). In the latter, sedimentation consisted mainly on alluvial fan/fan delta and lacustrine delta deposits passing eastward toward more distal lacustrine environments dominated by turbiditic and fan/lobe systems. Along the western border of the Yarkand-Fergana Basin, the existence of several basement highs is attested by the presence of angular unconformities between Lower Jurassic alluvial fan/delta fan systems and the Paleozoic basement rocks (e.g. in Terek or in Kara-Alma regions). The exposed tectonic structures within the north Yarkand-Fergana region are complex, including folds and NW-SE trending faults systems (Fig. 7). In this area, these faults

are associated with changes in thickness and in facies of the Lower Jurassic sequences suggesting that first-order fault zones controlled sedimentation during this period (Tseyler et al., 1982). In the south Yarkand-Fergana Basin, Lower-Middle Jurassic sediment thickness decreases away from the Talas-Fergana Fault (Sobel, 1999) suggesting half-graben geometry (Sinitsyn, 1960) (Fig. 16B).

The Early Jurassic corresponds to a period of renewed transtensive tectonic activity along the Talas Fergana/Karatau Fault which led to the opening of the Yarkand-Fergana, Leontiev and South Turgay basins (Sobel et al., 1999; Moseley and Tsimmer, 2000; Allen et al., 2001; Shi et al., 2016; Alexeiev et al., 2017; Schnyder et al., 2017). However, the precise timing of opening of these basins is not clearly known. In the South Turgay Basin, no biostratigraphic ages are available while in the Leontiev Basin, Lower Jurassic sediments have a pre-Toarcian (Pliensbachian) to Toarcian age (Schnyder et al., 2017). Within the Yarkand-Fergana Basin, we have identified the oldest palynomorph assemblages as Early Jurassic (Sinemurian?) to Pliensbachian in age (Table S2). Altogether these data seems to support a Sinemurian to Pliensbachian age of opening of the Yarkand-Fergana and Leontiev basins (and probably of the Turgay Basin) but further studies are needed to confirm this hypothesis.

Meanwhile, to the west, in the Fergana Basin, renewed sedimentation also occurred during the Early Jurassic leading to the accumulation of 90–400 m-thick alluvial to lacustrine deposits (Osmonbetov et al., 1982; Clarke, 1984; De Pelsmaeker et al., 2018). In this basin, lateral thickness variations are minor, suggesting a different style of formation (Bande et al., 2017b) compared to the Yarkand-Fergana Basin (Fig. 16B).

Finally, this period is also characterized by tectonic reactivation of Paleozoic structures and exhumation within the Kyrgyz Tian Shan identified by low-temperature thermochronology (Sobel et al., 2006; De Grave et al., 2007, 2011; Nachtergaele et al., 2018).

However, this tectonic activity only led to localized relief building in the Tian Shan region (Morin et al., 2018 and references within). Lower Jurassic sedimentation also occurred within restricted areas of the Kyrgyz Tian Shan (De Pelsmaeker et al., 2018) and it is not clear if the Talas-Fergana/Karatau fault acted as a barrier or if the Yarkand-Fergana Basin expanded further east. Although we investigated only one location along the Talas Fergana Fault, we did not find any evidence of westward directed sediment flux as could be expected should the fault form a major scarp.

### 5.3. Late Pliensbachian–Middle Jurassic

In the northern Yarkand-Fergana Basin, late Pliensbachian to Middle Jurassic sedimentary rocks are characteristic of more distal depositional environments compared to those previously described (Fig. 16C). Indeed, sedimentation consisted mainly of lacustrine delta, lacustrine and distal lacustrine deposits often associated with extensive coal layers (this study; De Pelsmaeker et al., 2018). Some basement highs could still have been present but generally, this period corresponded to a widening of the Yarkand-Fergana Basin (Fig. 16C). Late Early–Middle Jurassic motion along the Talas-Fergana fault still occurred leading to continuous opening and sedimentation within the South Turgay, Leontiev and Yarkand Fergana basins (Sobel, 1999; Moseley and Tsimmer, 2000; Allen et al., 2001; Shi et al., 2016; Alexeiev et al., 2017; Schnyder et al., 2017).

To the west, in the Fergana Basin, Middle Jurassic sedimentation consisted of 100 to 300 m-thick alluvial to lacustrine deposits often associated to coal beds (Clarke, 1988; De Pelsmaeker et al., 2018).

Finally, in the Kyrgyz Tian Shan, this period was characterized by slow erosion leading to progressive exhumation of the basement areas (Morin et al., 2018 for a synthesis). Meanwhile, no sedimentation occurred within the Kyrgyz Tian Shan during this period as attested by the presence of a Middle Jurassic to Eocene hiatus (VNIGNI et al., 1992).

#### 5.4. Late Jurassic–Early Cretaceous:

In the north Yarkand-Fergana Basin, no Upper Jurassic–Early Cretaceous sediment has been observed while along the eastern Fergana Basin margin, sedimentation consisted mainly of alluvial fan and alluvial plain deposits (Fig. 16D). Although in the Yassi River section presented in this study, the Late Jurassic–Early Cretaceous conglomerates mainly contain Paleozoic rock fragments, provenance studies on similar series from the NE Fergana Basin (Tash Komyr section) indicate potential recycling of older Jurassic sediments and a smaller drainage area compared to the Early–Middle Jurassic paleogeography (De Pelsmaeker et al., 2018). Poyarkova (1969) noted that in the eastern Fergana Basin, the Early Cretaceous series, mainly containing pebbles derived from Paleozoic basement rocks, rested without angular unconformity on the Jurassic deposits. However, such an unconformity has been observed in the southern Fergana Basin (Gabril'yan and Babayev, 1960). These various observation may indicate that, like in the Chinese Tian Shan, angular unconformities could develop locally (Jolivet et al., 2017). The preponderance in the Late Jurassic–Early Cretaceous conglomerates of Paleozoic basement-derived clasts, associated to minor Mesozoic sandstone fragments suggest an inversion of the Yarkand-Fergana Basin during that period. Tectonic inversion and deformation have also been described in the South Turgay (Yin et al., 2012) and Leontiev basins (Allen et al., 2001) indicating that transpression occurred along the Talas-Fergana/Karatau fault during this period. This is attested by low-temperature thermochronology which identifies a Late Jurassic–Early Cretaceous cooling event in the Kyrgyz Tian Shan Range suggesting localized relief building (De Grave et al., 2007, 2011, 2013; Glorie and De Grave., 2016; Nachtergaele et al., 2018).

## 6. Geodynamic implications and remaining uncertainties

The Early–Middle Jurassic corresponds to a peculiar period in the tectonic history of the Talas Fergana/Karatau Fault. Indeed, despite having undergone several phases of pure or transpressionnal dextral strike slip motion during its Paleozoic to Cenozoic evolution (Ognev, 1939; Sobel, 1999; Allen et al., 2001; Alexeiev et al., 2009, 2017; Rolland et al., 2013), only its Jurassic activity led to the opening of several associated sedimentary basins (i.e. South Turgay, Leontiev and Yarkand-Fergana basins). However, the driving mechanism leading to these transient transtensional kinematics is still unclear. Some studies proposed that Early–Middle Jurassic strike-slip activity was driven by a regional compressional setting induced by the Qiangtang collision (Sobel, 1999). However, the Early–late Early Jurassic timing of opening of the Yarkand-Fergana Basin does not seem to be in agreement with this hypothesis. The final stage of the Qiangtang collision is dated to the Late Triassic–Early Jurassic, with the emplacement, in Eastern Tibet of late-orogenic to post-orogenic granites around 200 Ma (Zhang et al., 2006; Roger et al., 2010). If associated to the Qiangtang collision, the strike-slip motion along the Talas Fergana/Karatau Fault would thus be contemporaneous of the very final collision phase. Furthermore, the subsequent Jurassic to Early Cenozoic period was marked, in Tibet, by an absence of vertical tectonic movements (Roger et al., 2011; Jolivet, 2017), except for the late Early Cretaceous Lhasa collision in southern Tibet (Kapp et al., 2005, 2007). This again contradicts the Pliensbachian–Middle Jurassic ongoing transtension in the Yarkand-Fergana Basin being related to tectonic events within the Tibet region. Other studies proposed that this Early–Middle Jurassic strike-slip activity could have occurred in a regional extensional setting (Alexeiev et al., 2017; Morin et al., 2018). Indeed, as indicated above, no major collisional event has been identified along the Eurasian margin during this period while simultaneous widespread extension associated to back-arc opening along the northern Neo-Tethys subduction zone affected the Caspian/Turan domain to the west

(Zonenshain and Pichon, 1986; Nikishin et al., 1998; Thomas et al., 1999; Brunet et al., 2003, 2017; Robert et al., 2014; Mordvintsev et al., 2017; Rolland et al., 2020). It is for example largely accepted that the South Caspian Basin initiated as a back-arc structure during the Early(?) to Middle Jurassic (Brunet et al., 2003 and references therein). Magmatism associated to the subduction has been identified in the Transcaucasus (with a first peak activity during bajocian – Bathonian) and Pontide regions, west of the South Caspian Basin (Yilmaz et al., 1997; Nikishin et al., 2001; Brunet et al., 2003). As illustrated on Figure 17, this extension reactivated mainly NW–SE orientated Paleozoic structures as normal faults. In turn, these normal faults induced localized subsidence leading to the emplacement of elongated NW–SE depocenters in the Amu-Darya and Kopet Dag basins (e.g. Robert et al., 2014; Brunet et al., 2017; Mordvintsev et al., 2017). The evolution and geometry of these basins are similar to those observed in the northern Yarkand-Fergana Basin: a half-graben controlled by a NW–SE oriented tectonic structure corresponding to the Talas-Fergana/Karatau fault. However, further work is needed to support this hypothesis and to better constrain the evolution of the whole Yarkand-Fergana Basin. Following that second model, the Early–Middle Jurassic Talas Fergana/Karatau Fault would thus represent the easternmost reach of the extensional deformation-field controlled by the Neo-Tethys subduction (Fig. 17; Morin et al., 2018).

Several questions still remain. For example, if following the extension model, how is the stress transmitted for more than 1000 km away from the subduction zone? Again, the exact timing of the Late Jurassic–Early Cretaceous inversion of the Yarkand-Fergana Basin is poorly constrained and the associated driving mechanism remains unknown. Low-magnitude compression occurred throughout many ranges in Central Asia without consensus on the geodynamic setting (Jolivet, 2017 and references therein). These questions are largely linked to the difficulty in dating the deposits (mainly conglomerates) associated to this event



(Hendrix et al., 1992; Eberth et al., 2001; Wang et al., 2013; Jolivet et al., 2017; Morin et al., 2018). Only one mafic sill intruded in the dated at  $144 \pm 8$  Ma (U-Pb on apatite) Hodzhiabad Fm. in the Tash Komyr section (NE Fergana Basin) provide a minimum age for these deposits.

## 7. Conclusions

The sedimentological, palynological and structural data presented in this study provide new constraints on the tectono-stratigraphic evolution of the Yarkand-Fergana Basin.

(1) During the Middle–Late Triassic, the north Yarkand-Fergana and north-east Fergana basins are dominated by erosion.

(2) The Early Jurassic Sinemurian(?)–Pliensbachian marks the onset of sedimentation, at least in the northern Yarkand-Fergana Basin. At that time, renewed activity along the Talas-Fergana/Karatau fault led to the opening of the Yarkand-Fergana Basin as a half-graben. However, this timing does not favor the idea of a tectonic reactivation induced by the Qiangtang collision and favor the hypothesis of Neo-Tethys subduction related extension affecting the entire Caspian-Turan domain to the west.

(3) Continuous opening of the Yarkand-Fergana Basin occurred during the late Early – Middle Jurassic probably related to ongoing subduction-related extension along the northern Neo-Tethys margin.

(4) Finally, the Late Jurassic–Early Cretaceous corresponds to a period of renewed tectonic activity in the area leading to the inversion of the north Yarkand-Fergana Basin.

Further work on the Yarkand-Fergana Basin is needed to better constrain the geodynamic mechanism and stress-field that led to its opening during the Early–late Early Jurassic as well as those that led to Late Jurassic–Early Cretaceous inversion.

**Acknowledgments**

We thank Anatoliy Rybin, Director of the Research Station of the Russian Academy of Sciences in Bishkek, as well as Evgeniy Ispolinov and Alexander Dzalba for logistic support during the work in Tian Shan. This study was supported by a CASP Fieldwork Research Award and by an Innovating Science Grant for PhD students awarded by Geosciences Rennes. We thank the reviewers Y.S. Biske and Y. Rolland for their very useful and constructive comments to the initial version of this work and Associate Editor I. Safonova for handling the manuscript.

**References**

- Alexeiev, D.V., Bykadorov, V.A., Volozh, Yu.A., Sapozhnikov, R.B., 2017. Kinematic analysis of Jurassic grabens of Southern Turgai and the role of the Mesozoic stage in the evolution of the Karatau–Talas–Ferghana strike-slip fault, Southern Kazakhstan and Tian Shan. *Geotectonics*, 51 (2), 105–120.
- Alexeiev, D.V., Cook, H.E., Buvtyshkin, V.M., Golub, L.Y., 2009. Structural evolution of the Ural–Tian Shan junction: A view from Karatau ridge, South Kazakhstan. *Comptes Rendus Geoscience*, 341(2-3), 287-297.
- Allen, M.B., Alsop, G.I., Zhemchuzhnikov, V.G., 2001. Dome and basin refolding and transpressive inversion along the Karatau fault System, southern Kazakhstan. *Journal of the Geological Society of London*, 158, 83–95.
- Bande, A., Sobel, E.R., Mikolaichuk, A., Acosta, V.T., 2017a. Talas–Fergana Fault Cenozoic timing of deformation and its relation to Pamir indentation. *Geological Society, London, Special Publications*, 427(1), 295-311.
- Bande, A., Radjabov, S., Sobel, E.R., Sim, T., 2017b. Cenozoic palaeoenvironmental and tectonic controls on the evolution of the northern Fergana Basin. *Geological Society, London, Special Publications*, 427(1), 313-335.
- Bazhenov, M.L., Chauvin, A., Audibert, M., Levashova, N.M., 1993. Permian and Triassic paleomagnetism of the south-west Tien Shan: the timing and mode of tectonic rotations. *Earth and Planetary Science Letters*, 118, 195–212.
- Bazhenov, M.L., Burtman, V.S., Dvorova, A.V., 1999. Permian paleomagnetism of the Tien Shan fold belt, Central Asia: post-collisional rotations and deformation. *Tectonophysics*, 312(2-4), 303-329.

- 639 Belgovskiy G.L., Ektova L.A., Maslova E.V., 1958. Explanation note to the sheet K-43-  
640 XXXIII of the Geological map of USSR, scale 1:200 000, 106 p. (in Russian).
- 641 Bhattacharya, J.P., 2010. Deltas. In: James, N.P., Dalrymple, R.W. (Eds.), *Facies Models* 4.  
642 Geological Association of Canada, *GEOtext*. pp. 233–264.
- 643 Biske, Y.S., Porshnyakov, G.S., Talashmanov, Y.A., 1982. Hercynides of the Ferghana Range  
644 and adjacent regions of the Southern Tianshan. *Leningrad University*, Leningrad (in Russian).
- 645 Burtman, V.S., 1964. The Talaso-Fergana strike-slip fault. *Tr. Geol. Inst. Akad. Nauk*  
646 *USSR*, 104, 143.
- 647 Burtman, V.S., Skobelev, S. F., Molnar, P., 1996. Late Cenozoic slip on the Talas-Ferghana  
648 fault, the Tien Shan, central Asia. *Geological Society of America Bulletin*, 108(8), 1004-1021.
- 649 Burtman, V.S., 2012. Geodynamics of Tibet, Tarim, and the Tien Shan in the Late Cenozoic.  
650 *Geotectonics*, 46(3), 185-211.
- 651 Bujak, J.P., Williams, G.L., 1977. Jurassic palynostratigraphy of offshore eastern  
652 Canada. *Developments in Palaeontology and Stratigraphy* 6, 321-339.
- 653 Brick, M.I., 1953. The Mesozoic flora of eastern Fergana coal basin. *Gosgeolizdat Publishing*  
654 *House, Moscow*, 112p. (in Russian).
- 655 Brunet, M.F., Korotaev, M.V., Ershov, A.V., Nikishin, A.M., 2003. The South Caspian Basin:  
656 a review of its evolution from subsidence modelling. *Sediment. Geol.*, 156 (1), 119–148.
- 657 Brunet, M.F., Ershov, A.V., Korotaev, M.V., Melikhov, V.N., Barrier, E., Mordvintsev, D.O.,  
658 Sidorova, I.P., 2017. Late Palaeozoic and Mesozoic evolution of the Amu Darya Basin  
659 (Turkmenistan, Uzbekistan). *Geological Society London Special Publication*, 427 (1), 89–  
660 144.

- Clarke, J.W., 1984. Geology and possible uranium deposits of the Fergana region of Soviet Central Asia (No. 84-513). US Geological Survey.
- De Grave, J., Buslov, M.M., Van den Haute, P., 2007. Distant effects of India-Eurasia convergence and Mesozoic intracontinental deformation in Central Asia: Constraints from apatite fission-track thermochronology. *Journal of Asian Earth Sciences* 29, 188-204.
- De Grave, J., Glorie, S., Buslov, M.M., Izmer, A., Fournier-Carrie, A., Batalev, V.Y., Vanhaecke, F., Elburg, M., Van den haute, P., 2011. The thermo-tectonic history of the Song-Kul plateau, Kyrgyz Tien Shan: constraints by apatite and titanite thermochronometry and zircon U/Pb dating. *Gondwana Research* 20(4), 745-763.
- De Grave, J., Glorie, S., Buslov, M.M., Stockli, D.F., McWilliams, M.O., Batalev, V.Y., Van den Haute P., 2013. Thermo-tectonic history of the Issyk-Kul basement (Kyrgyz Northern Tien Shan, Central Asia). *Gondwana Research* 23, 998-1020.
- De Pelsmaecker, E., Jolivet, M., Laborde, A., Poujol, M., Robin, C., Zhimulev, F.I., Nachtergaele, S., Glorie, S., De Clercq, S., Batalev, V.Y., De Grave, J., 2018. Source-to-sink dynamics in the Kyrgyz Tien Shan from the Jurassic to the Paleogene: Insights from sedimentological and detrital zircon U-Pb analyses. *Gondwana Research* 54, 180-204.
- Eberth, D.A., Brinkman, D.B., Chen, P.-J., Yuan, F.-T., Wu, S.-Z., Li, G., Cheng, X.-S., 2001. Sequence stratigraphy, paleoclimate patterns, and vertebrate fossil preservation in Jurassic-Cretaceous strata of the Junggar Basin, Xinjiang Autonomous Region, People's Republic of China. *Canadian Journal of Earth Sciences* 38, (12), 1627–1644.
- Feld, C., Haberland, C., Schurr, B., Sippl, C., Wetzel, H.-A., Roessner, S., Ickrath, M., Abdybachaev, U., Orunbaev, S., 2015. Seismotectonic study of the Fergana Region (Southern Kyrgyzstan): distribution and kinematics of local seismicity. *Earth, Planets and Space* 67, 1-13.

- 685 Gabril'yan, A.M., Babayev, A.G., 1960. Basic geologic premises regarding the oil and gas  
686 potentialities of Uzbekistan. *Izvestiya Akademii Nauk SSSR, Seriya Geologicheskaya*, 9, 45-  
687 51.
- 688 Genkina, R.Z., 1977. Stratigraphy of Jurassic continental rocks of the Fergana Range and  
689 paleobotanic substantiation of their age. *Sovetskaya Geologia* 9, 61-79 (in Russian).
- 690 Glorie, S., De Grave, J., 2016. Exhuming the Meso-Cenozoic Kyrgyz Tianshan and Siberian  
691 Altai-Sayan: A review based on low-temperature thermochronology. *Geoscience Frontiers* 7,  
692 155-170.
- 693 Hendrix, M.S., Graham, S.A., Carroll, A.R., Sobel, E.R., McKnight, C.L., Schulein, B.J.,  
694 Wang, Z., 1992. Sedimentary record and climatic implications of recurrent deformation in the  
695 Tien Shan: evidence from Mesozoic strata of the north Tarim, south Junggar, and Turpan  
696 basins, Northwest China. *Geological Society of America Bulletin* 104 (1), 53–79.
- 697 Hinds, D.J., Aliyeva, E., Allen, M.B., Davies, C.E., Kroonenberg, S.B., Simmons, M.D.,  
698 Vincent, S.J., 2004. Sedimentation in a discharge dominated fluvial–lacustrine system: the  
699 Neogene Productive Series of the South Caspian Basin, Azerbaijan. *Marine and Petroleum*  
700 *Geology* 21 (5), 613–638.
- 701 Jolivet, M., 2017. Mesozoic tectonic and topographic evolution of Central Asia and Tibet: a  
702 preliminary synthesis. *Geological Society of London Special Publication* 427 (1), 19–55.
- 703 Jolivet M., Bourquin S., Heilbronn G., Robin C., Barrier L., Dabard M-P., Jia Y., De  
704 Pelsmaeker E., Fu B., 2017. The Upper-Jurassic – Lower Cretaceous alluvial-fan deposits of  
705 the Kalaza Formation (Central Asia): tectonic pulse or increased aridity? *Geological Society*  
706 *of London Spec. Pub.* 427, <http://doi.org/10.1144/SP427.6>

- 707 Jourdon, A., Petit, C., Rolland, Y., Loury, C., Bellahsen, N., Guillot, S., Le Pourhiet, L.,  
 708 Ganino, C., 2017. New structural data on Late Paleozoic tectonics in the Kyrgyz Tien Shan  
 709 (Central Asian Orogenic Belt). *Gondwana Research* 46, 57-78.
- 710 Kapp, P., Yin, A., Harrison, T.M., Ding, L., 2005. Cretaceous–Tertiary shortening, basin  
 711 development, and volcanism in central Tibet. *Geological Society of America Bulletin* 117,  
 712 865–878.
- 713 Kapp, P., DeCelles, P. G., Gehrels, G. E., Heizler, M., Ding, L., 2007. Geological records of  
 714 the Lhasa-Qiangtang and Indo-Asian collisions in the Nima area of central Tibet. *Geological*  
 715 *Society of America Bulletin* 119, 917–932.
- 716 Konopelko, D., Seltnann, R., Apayarov, F., Belousova, E., Izokh, A., Lepekhina, E., 2013.  
 717 U–Pb–Hf zircon study of two mylonitic granite complexes in the Talas-Fergana fault zone,  
 718 Kyrgyzstan, and Ar–Ar age of deformations along the fault. *Journal of Asian Earth*  
 719 *Sciences* 73, 334-346.
- 720 Korjenkov, A.M., Rust, D., Tibaldi, A., Abdieva, S.V., 2012. Parameters of the strong  
 721 Paleoeearthquakes along the Talas-Fergana fault, the Kyrgyz Tien Shan. In: *Earthquake*  
 722 *Research and Analysis-Seismology, Seismotectonic and Earthquake Geology*. InTech.
- 723 Korzhenkov, A.M., Rogozhin, E.A., Shen, X.H., Tian, Q.J., Xu, Y.R., 2014. Strong  
 724 paleoeearthquakes along the Talas-Fergana Fault, Kyrgyzstan. *Geodesy and Geodynamics* 5  
 725 (1), 11-19.
- 726 Loury, C., Rolland, Y., Cenki-Tok, B., Lanari, P., Guillot, S., 2016. Late Paleozoic evolution  
 727 of the South Tien Shan: Insights from P–T estimates and allanite geochronology on  
 728 retrogressed eclogites (Chatkal range, Kyrgyzstan). *Journal of Geodynamics* 96, 62-80.

- 729 Loury, C., Rolland, Y., Guillot, S., Lanari, P., Ganino, C., Melis, R., Jourdon, A., Petit, C.,  
730 Beyssac, O., Gallet, S., Monié, P., 2018a. Tectonometamorphic evolution of the Atbashi  
731 high-P units (Kyrgyz CAO, Tien Shan): Implications for the closure of the Turkestan  
732 Ocean and continental subduction–exhumation of the South Kazakh continental margin.  
733 *Journal of Metamorphic Geology* 36(8), 959-985.
- 734 Loury, C., Rolland, Y., Lanari, P., Guillot, S., Bosch, D., Ganino, C., Jourdon, A., Petit, C.,  
735 Gallet, S., Monié, P., Riel, N., 2018b. Permian charnockites in the Pobeda area: Implications  
736 for Tarim mantle plume activity and HT metamorphism in the South Tien Shan range. *Lithos*  
737 304-307, 135-154.
- 738 Luik A.A., Zapolnov A.K., 1960. Geological map: K-43-XXVII. Geological map of the  
739 USSR. Alay-Kakshaalskaya series, scale: 1: 200000. In: Zubtsov, E.I. (Ed.), Department of  
740 Geology and Protection of Natural Resources at the SovMin of the Kirghiz SSR.
- 741 Marshall, J.D., 2000. Sedimentology of a Devonian fault-bounded braidplain and lacustrine  
742 fill in the lower part of the Skrinkle Sandstones, Dyfed, Wales. *Sedimentology*, 47 (2), 325–  
743 342.
- 744 Miall, A.D., 1978. Lithofacies types and vertical profile models in braided river deposits: a  
745 summary. In: Miall, A.D. (Eds.), *Fluvial Sedimentology*. Canadian Society Petroleum  
746 Geology, Memoirs, 5, 597–604.
- 747 Miall, A.D., 1996. *The Geology of Fluvial Deposits*. Springer, Berlin, 582 p.
- 748 Moisan, P., Voigt, S., Pott, C., Buchwitz, M., Schneider, J. W., Kerp, H., 2011. Cycadalean  
749 and bennettitalean foliage from the Triassic Madygen Lagerstätte (SW Kyrgyzstan, central  
750 Asia). *Review of Palaeobotany and Palynology*, 164(1-2), 93-108.



- 751 Mordvintsev, D., Barrier, E., Brunet, M.F., Blanpied, C., Sidorova, I., 2017. Structure and  
 752 evolution of the Bukhara-Khiva region during the Mesozoic: the northern margin of the Amu-  
 753 Darya Basin (southern Uzbekistan). *Geological Society London, Special Publication*, 427,  
 754 SP427–16.
- 755 Morin, J., Jolivet, M., Robin, C., Heilbronn, G., Barrier, L., Bourquin, S., Jia, Y., 2018.  
 756 Jurassic paleogeography of the Tian Shan: An evolution driven by far-field tectonics and  
 757 climate. *Earth-Science Reviews*, 187, 286-313.
- 758 Moseley, B.A., Tsimmer, V.A., 2000. Evolution and hydrocarbon habitat of the South Turgay  
 759 Basin, Kazakhstan. *Petroleum Geoscience*, 6 (2), 125-136.
- 760 Nachtergaele, S., De Pelsmaeker, E., Glorie, S., Zhimulev, F., Jolivet, M., Danišík, M.,  
 761 Buslov, M.M., De Grave, J., 2018. Meso-Cenozoic tectonic evolution of the Talas-Fergana  
 762 region of the Kyrgyz Tien Shan revealed by low-temperature basement and detrital  
 763 thermochronology. *Geoscience Frontiers*, 9(5), 1495-1514.
- 764 Nikishin, A.M., Cloetingh, S.A.P.L., Brunet, M.F., Stephenson, R.A., Bolotov, S.N., Ershov,  
 765 A.V., 1998. Scythian Platform, Caucasus and Black Sea Region: Mesozoic–Cenozoic  
 766 Tectonic History and Dynamics. *Peri-Tethys Memoir*, 3, 163–176.
- 767 Nikishin, A., Ziegler, P.A., Panov, D.I., Nazarevich, B.P., Brunet, M.-F., Stephenson, R.A.,  
 768 Bolotov, S.N., Korotaev, M.V., Tikhomirov, P.L., 2001. Mesozoic and Cenozoic evolution of  
 769 the Scythian Platform – Black-Sea – Caucasus domain. In: Ziegler, P.A., Cavazza, W.,  
 770 Robertson, A.H.F., Crasquin-Soleau, S. (Eds.), *Peri-Tethys Memoir 6: Peri-Tethyan*  
 771 *Rift/Wrench Basins and Passive Margins. Mémoires du Muséum d'Histoire Naturelle de*  
 772 *Paris*, 186, 295–346.
- 773 Nikolaev, V.A., 1933. On the most important structural line of the Tien-Shan. *Zapiski*  
 774 *Vserossiyskogo Mineralogicheskogo Obshestva*, 2, 347-354.

- 775 Ognev, V.N., 1939. Talas-Fergana Fault. *Izvestiya Akademiia Nauk SSSR, Seriya*  
 776 *Geologicheskaya*, 4, 71-79 (in Russian).
- 777 Ognev, V.N., 1946. The Structural and facies characteristics of the coal-bearing strata in the  
 778 eastern Fergana coal Basin. *Frunze, Izvestia Kirgiz. Filiala, Akademiia Nauk SSSR* (in  
 779 Russian).
- 780 Osmonbetov, K.O. (Ed.), 1980. Geological Map of the Kyrgyz SSR, Scale 1:500000.  
 781 *VSEGEI, Leningrad* (in Russian).
- 782 Osmonbetov, K.O., Knauf, V.I., Korolyov, V.G. (Eds.), 1982. Stratified and intrusive  
 783 formations of Kyrgyzstan, Book 1. *Ilim, Frunze* (in Russian).
- 784 Pollard, J.E., Steel, R.J., Undersrud, E., 1982. Facies sequences and trace fossils in  
 785 lacustrine/fan delta deposits, Hornelen Basin (M. Devonian), Western Norway. *Sedimentary*  
 786 *Geology*, 32 (1–2), 63–87.
- 787 Postma, G., 1990. Depositional architecture and facies of river and fan deltas: a synthesis. In:  
 788 Collella, A., Prior, D.B. (Eds.), Coarse-grained deltas. *International Association of*  
 789 *Sedimentologists, Special Publications*, 10, 13-27.
- 790 Poyarkova Z.N., 1969. Stratigraphy of the Cretaceous beds of southern Kyrgyzstan. *Ilym,*  
 791 *Frunze* (In Russian).
- 792 Reynolds, A.D., Simmons, M.D., Bowman, M.B.J., Henton, J., Brayshaw, A.C., Ali-Zade,  
 793 A.A., Guliyev, I.S., Suleymanova, S.F., Ateava, E.Z., Mamedova, D.N., Koshkarly, R.O.,  
 794 1982. Implications of outcrop geology for reservoirs in the Neogene Productive Series:  
 795 Apsheron Peninsula, Azerbaijan. *AAPG Bulletin*, 82, 25–49.

- 796 Rizza, M., Abdrakhmatov, K., Walker, R., Braucher, R., Guillou, V., Carr, A.S., Campbell,  
797 G., McKenzie, D., Jackson, J., Aumaître, G., Bourlès, D.L., Keddadouche, K., 2019. Rate of  
798 slip from multiple Quaternary dating methods and paleoseismic investigations along the  
799 Talas-Fergana Fault: Tectonic implications for the Tien Shan Range. *Tectonics*, 38(7), 2477-  
800 2505, doi:org/10.1029/2018TC005188.
- 801 Robert, A.M., Letouzey, J., Kavoosi, M.A., Sherkati, S., Müller, C., Vergés, J., Aghababaei,  
802 A., 2014. Structural evolution of the Kopeh Dagh fold-and-thrust belt (NE Iran) and  
803 interactions with the South Caspian Sea Basin and Amu Darya Basin. *Marine and Petroleum*  
804 *Geology*, 57, 68–87.
- 805 Roger F., M. Jolivet, J. Malavieille., 2010. The tectonic evolution of the Songpan Garzê  
806 (North Tibet) and adjacent areas from Proterozoic to Present: a synthesis. *Journal of Asian*  
807 *Earth Sciences*, 39, 254-269.
- 808 Roger F., Jolivet M., Cattin R., Malavieille J., 2011. Mesozoic-Cenozoic tectonothermal  
809 evolution of the eastern part of the Tibetan plateau (Songpan-Garzê, Longmen Shan area):  
810 insights from thermochronological data and simple thermal modeling. *Geological Society of*  
811 *London Special Publications*, 353, 9-25.
- 812 Rolland, Y., Alexeiev, D. V., Kröner, A., Corsini, M., Loury, C., Monié, P., 2013. Late  
813 Palaeozoic to Mesozoic kinematic history of the Talas–Ferghana strike-slip fault (Kyrgyz  
814 West Tianshan) as revealed by  $^{40}\text{Ar}/^{39}\text{Ar}$  dating of syn-kinematic white mica. *Journal of*  
815 *Asian Earth Sciences*, 67, 76-92.
- 816 Rolland, Y., Hässig, M., Bosch, D., Bruguier, O., Melis, R., Galoyan, G., Topuz, G.,  
817 Sahakyan, L., Avagyan, A., Sosson, M., 2020. The East Anatolia–Lesser Caucasus ophiolite:  
818 An exceptional case of large-scale obduction, synthesis of data and numerical modelling.  
819 *Geoscience Frontiers* 11, 83-108

- 820 Schnyder, J., Pons, D., Yans, J., Tramoy, R., Abdulanova, S., 2017. Integrated stratigraphy of  
 821 a continental Pliensbachian–Toarcian boundary (lower Jurassic) section at Taskomirsay,  
 822 leontiev graben, southwest Kazakhstan. *Geological Society, London, Special*  
 823 *Publications*, 427(1), 337-356.
- 824 Shi, J., Jin, Z., Fan, T., Liu, Q., Zhang, F., Fan, X., 2016. Sequence development, depositional  
 825 filling evolution, and prospect forecast in northern Arysium Depression of South Turgay  
 826 Basin, Kazakstan. *Energy Exploration & Exploitation*, 34 (4), 621-642.
- 827 Sinitsyn, N.M., 1960. Tectonics of the mountain framing of Fergana. *Publishing House of*  
 828 *Leningrad University, Leningrad*.
- 829 Sobel, E.R., 1999. Basin analysis of the Jurassic-Lower Cretaceous southwest Tarim Basin,  
 830 northwest China. *Geological Society of America Bulletin*, 111 (5), 709-724.
- 831 Sobel, E.R., Chen, J., Heermance, R.V., 2006. Late Oligocene – Early Miocene initiation of  
 832 shortening in the Southwestern Chinese Tian Shan: implications for Neogene shortening rate  
 833 variations. *Earth and Planetary Science Letters*, 247, 70-81.
- 834 Svendsen, J., Stollhofen, H., Krapf, C.B.E. Stanistreet, I.G., 2003. Mass and  
 835 hyperconcentrated flow deposits record dune damming and catastrophic breakthrough of  
 836 ephemeral rivers, Skeleton Coast Erg, Namibia. *Sedimentary Geology*, 160, 7–31.
- 837 Thomas, J.C., Cobbold, P.R., Shein, V.S., Le Douaran, S., 1999. Sedimentary record of late  
 838 Paleozoic to recent tectonism in Central Asia—analysis of subsurface data from the Turan and  
 839 south Kazak domains. *Tectonophysics*, 313 (3), 243–263.
- 840 Tibaldi, A., Corazzato, C., Rust, D., Bonali, F.I., Pasquare Mariotto, F.A., Korzhenkov, A.M.,  
 841 Oppizzi, P., Bonzanigo, I., 2015. Tectonic and gravity-induced deformation along the active  
 842 Talas-Fergana Fault, Tien Shan, Kyrgyzstan. *Tectonophysics*, 657, 38-62.

- 843 Trifonov, V.G., Korzhenkov, A.M., Omar, K.M., 2015. Recent geodynamics of major strike-  
844 slip zones. *Geodesy and Geodynamics*, 6(5), 361-383.
- 845 Tseysler, V.M., Florenskiy, V.S., Vasyukov, V.S., Turov, A.V., 1982. Tectonic structures of  
846 the northern Fergana Range. *International Geology Review*, 24, 881–890.
- 847 Verzhilin, N.N., 1968. On the problem of the Talas-Ferghana strike-slip fault. *In: Ognev, V.N.*  
848 *(Ed.) Problems of Regional Geology. Leningrad University, Leningrad, 67-70 (in Russian).*
- 849 VNIGNI and Beicip Franlab, 1992. Petroleum Potential of Central Asia. Rueil-Malmaison,  
850 France.
- 851 Wang J.H., Wang H., Chen H.H., Jiang S., Zhao S.E., 2013. Response of two lithosomes of  
852 Lower Cretaceous coarse clastic rocks to tectonism in Kuqa foreland sub-basin, Northern  
853 Tarim Basin, Northwest China. *Sedimentary Geology*, 289, 182-193.
- 854 Yilmaz, Y., Tüysüz, O., Yigitbas, E., Can Genç, S., Sengör, A.M.C., 1997. Geology and  
855 tectonic evolution of the Pontides. *In: Robinson, A.G. (Ed.), Regional and Petroleum Geol-*  
856 *ogy of the Black Sea and Surrounding Region. American Association of Petroleum*  
857 *Geologists, Memoir*, 68, 183-226, Tulsa, Oklahoma.
- 858
- 859 Yin, W., Fan, Z.F., Zheng, J.Z., Yin, J.Q., Zhang, M.J., Sheng, X.F., Guo, J.J., Li, Q.Y., Lin,  
860 Y.P., 2012. Characteristics of strike-slip inversion structures of the Karatau fault and their  
861 petroleum geological significances in the South Turgay Basin, Kazakhstan. *Petroleum*  
862 *Science*, 9(4), 444-454.
- 863 Zhang, H.F., Zhang, B.R., Harris, N., Zhang, L., Chen, Y.L., Chen, N.S., Zhao, Z.D., 2006.  
864 U–Pb zircon SHRIMP ages, geochemical and Sr–Nd–Pb isotopic compositions of intrusive  
865 rocks from the Longshan–Tianshui area in the southeast corner of the Qilian orogenic belt,

866 China: constraints on petrogenesis and tectonic affinity. *Journal of Asian Earth Sciences*, 27,  
867 751–764.

868 Zonenshain, L.P., Pichon, X., 1986. Deep basins of the Black Sea and Caspian Sea as  
869 remnants of Mesozoic back-arc basins. *Tectonophysics*, 123 (1–4), 181–211.

870

871

## 872 **Figures captions**

873 **Figure 1.** General tectonic framework of the Tian Shan region and Jurassic deposits  
874 associated to the Talas Fergana/Karatau Fault. Y-F B: Yarkand-Fergana Basin; TFF: Talas  
875 Fergana/Karatau Fault; N.L.: Nikolaev Line; NTSF: North Tian Shan Fault; K: Kratau Range;  
876 T: Talas Range; F: Fergana Range; Ksh: Kokshaal Range; Ch: Chatkal Range.

877 **Figure 2.** Simplified geological map of the Yarkand Fergana region. TFF: Talas Fergana  
878 Fault; Ba: Bayman-Bet; Ch: Chitty; Ka: Kara-Alma; Kt: Kara Tuybe; Ku: Kuzigongsu; Py:  
879 Pychan; Te: Terek; Ya: Yassy.

880 **Figure 3.** Synthesis of the chronostratigraphic charts available for the Jurassic to Early  
881 Cretaceous series in the Yarkand-Fergana, Fergana, Leontiev and South Turgay basins.

882 **Figure 4.** Geological maps available for the north Yarkand-Fergana region, note the  
883 differences in interpretation between geological maps. A: 1/500,000 scale geological map  
884 (Osmonbetov, 1980); B: 1/200,000 scale geological map (Luik and Zapolnov, 1960); C:  
885 Zoom on the Kara-Alma, Kara-Tuybe, Chitty and Pychan areas and on the studied sections.

**Figure 5.** Uninterpreted and interpreted panorama picture of the Bayman-Bet area illustrating the fan-shaped geometry observed within Jurassic deposits and the unconformable contact with Paleozoic basement rocks.

**Figure 6.** Field picture illustrating the unconformable contact between Jurassic conglomerates and Paleozoic rocks (A) and an example of normal fault observed in the Kara-Alma area (B).

**Figure 7.** Panorma pictures illustrating the general tectonic deformation observed in the Chitty valley (A, B and C) and in the Pychan area (D, E and F). E, F: Uninterpreted and interpreted panorama picture showing the geometric relation between Lower Jurassic sedimentary rocks and the Paleozoic basement in the Pychan region.

**Figure 8.** Pictures illustrating the various Jurassic sedimentary facies of the north Yarkand-Fergana Basin. See Table 2 for the facies codes and descriptions. Pictures of facies respectively from: A, Kara-Alma section; B and C, Yassy section; D, East Chitty area; E, Terek section; F, West Chitty area; G: Bayman-Bet section; H, Pychan area; I and J, West Chitty section; K, Terek section.

**Figure 9.** Outcrop picture and associated sedimentary log of the Bayman-Bet section.

**Figure 10.** Sedimentary log of the Kara Alma and the Kara Tuybe sections in the Yarkand-Fergana Basin. Associated facies assemblages and their interpretation in term of depositional environments as in Table 2.

**Figure 11.** Palynology plates of representative pollens and spores of the Kara Alma and Chitty sections. The sample number and the England Finder reference are given for each specimen. (1) *Araucariacites australis* (Kara Alma Section, Y-18-1, N64/2). (2) *Callialasporites dampieri* (Chitty Section, D-36, U30). (3) *Callialasporites turbatus* (Chitty Section, D-36, S43/2). (4) *Callialasporites turbatus* (Chitty Section, D-40, O56). (5)

909 *Callialasporites turbatus* (Chitty Section, D-40, V46/4). (6) *Perinopollenites elatoides* (Chitty  
 910 Section, D-36, P50/2). (7) *Perinopollenites elatoides* (Chitty Section, D-36, P49). (8)  
 911 *Cerebropollenites mesozoicus* (Chitty Section, D-40, L32/2). (9) *Cerebropollenites*  
 912 *mesozoicus* (Chitty Section, D-40, K50/2). (10) *Cerebropollenites thiergartii* (Chitty Section,  
 913 D-60, N2). (11) *Cerebropollenites thiergartii* (Chitty Section Part 1, Db-4, K48/2). (12)  
 914 *Tsugaepollenites* sp. (Chitty Section Part 1, Db-4, X46/4). (13) *Classopollis* sp. (Chitty  
 915 Section, D-16, V53/4). (14) *Classopollis* sp. (Chitty Section, D-16, Q32/2). (15)  
 916 *Chasmatosporites* sp. (Kara Alma Section, Y-18-4, L45/2). (16) *Cycadopites granulatus* (Kara  
 917 Alma Section, Y-18-4, N55/3). (17) *Cycadopites minimus* (Chitty Section Part 1, Db-4,  
 918 N40/3). (18) *Cycadopites ovalis* (Chitty Section Part 1, Db-4, O39). (19) *Spheripollenites*  
 919 *psilatus* (Kara Alma Section, Y-18-7, P59/1). (20) *Quadraeculina* sp. (Kara Alma Section, Y-  
 920 18-7, M38). (21) *Quadraeculina* sp. (Chitty Section, D-76, N30/2). (22) *Alisporites grandis*  
 921 (Kara Alma Section, Y-18-5, O43). (23) *Alisporites* sp. (Chitty Section, D-40, N43/2). (24).  
 922 *Pityosporites* sp. (Chitty Section, D-40, P43). (25) *Podocarpidites* sp. (Chitty Section, D-40,  
 923 K50). (26) *Abiespollenites* sp. (Chitty Section, D-40, P50). (27) Poorly preserved *Bisaccate*  
 924 pollen (Chitty Section, D-8, F60/4). (28) Poorly preserved, reworked *Lunatisporites* sp.  
 925 (Chitty Section, D-8, T44). (29) Poorly preserved, reworked *Lueckisporites* sp. (Chitty  
 926 Section, D-8, L34). (30) *Eucommiidites granulosus* (Chitty Section Part 1, Db-4, W51/3). (31)  
 927 *Cyathidites* sp. (Chitty Section, D-36, S53). (32) *Cyathidites* sp. (Kara Alma Section, Y-18-1,  
 928 H36/3). (33) *Concavissimisporites* sp. (Chitty Section Part 1, Db-4, D35/3). (34)  
 929 *Gleicheniidites* sp. (Chitty Section Part 1, Db-4, Q36/4). (35) *Apiculatisporites ovalis* (Kara  
 930 Alma Section, Y-18-1, K54/3). (36) *Apiculatisporites ovalis* (Chitty Section, D-8, R40/3).  
 931 (37) *Baculatisporites* sp. (Chitty Section Part 1, Db-4, V35). (38) *Osmundacidites wellmanii*.  
 932 (Kara Alma Section, Y-18-1, C48). (39) *Neoraistrickia* sp. (Kara Alma Section, Y-18-1, S39).  
 933 (40) *Lycopodiumsporites austroclavatidites*. (Kara Alma Section, Y-18-7, J52/2). (41)



Lycopodiacidites sp. (Chitty Section Part 1, Db-4, W50/2). (42) Cingulizonates sp. (Chitty Section, D-16, R29/4). (43) Striatella sp. (Chitty Section, D-16, S50/4). (44) Striatella sp. (Chitty Section, D-36, J59). (45) Nevesisporites vallatus (Chitty Section Part 1, Db-4, D51/4). (46) Verrucosisporites sp. (Chitty Section Part 1, Db-4, F54/1). (47) Reworked Aratrisporites sp. (Chitty Section Part 1, Db-4, S52/3). (48) Reworked Aratrisporites sp. (Chitty Section Part 1, Db-4, L40/1). (49) Reduviasporonites sp. (Kara Alma Section, Y-18-2, V49/2). (50) Reduviasporonites sp. (Kara Alma Section, Y-18-2, H35).

**Figure 12.** Sedimentary log of the West and East Chitty sections in the Yarkand-Fergana Basin. Associated facies assemblages and their interpretation in term of depositional environments as in Table 2.

**Figure 13.** (A) Field pictures presenting the sedimentary facies and the associated sedimentary log observed in the Pychan region; (B) Panorama picture illustrating the unconformable contact between Jurassic sedimentary rocks and the Paleozoic basement.

**Figure 14.** Sedimentary log of the Terek section in the Yarkand-Fergana Basin. Associated facies assemblages and their interpretation in term of depositional environments as in Table 2.

**Figure 15.** Sedimentary log of the Yassy section in the Fergana Basin. Associated facies assemblages and their interpretation in term of depositional environments as in Table 2.

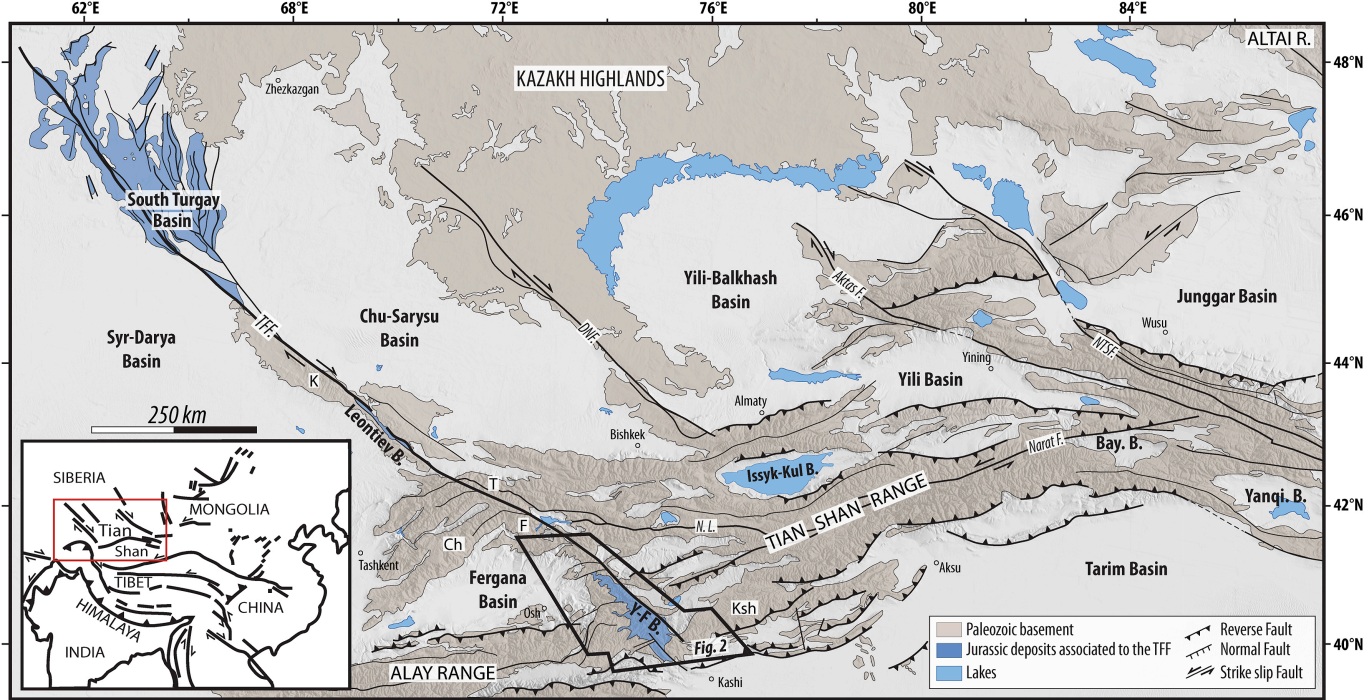
**Figure 16.** Schematic 3D blocks illustrating the Middle Triassic–Early Cretaceous tectono-stratigraphic evolution of the northern Yarkand-Fergana region.

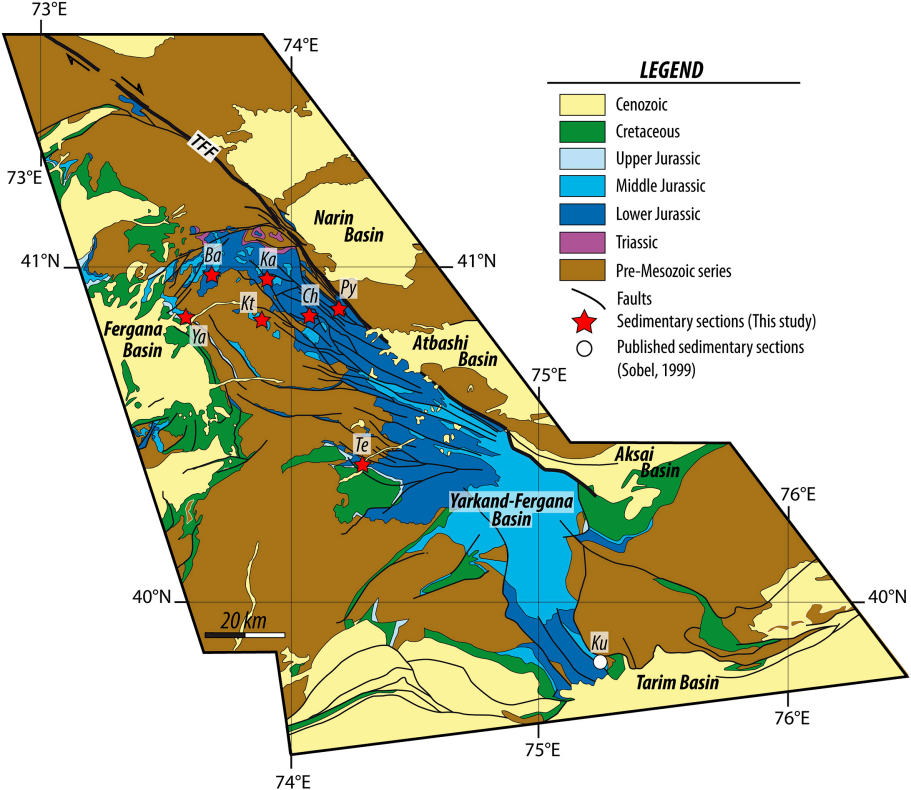
**Figure 17.** (A) Late Early to Middle Jurassic general geodynamic and paleotopographic framework of Asia (modified from Jolivet, 2017); EU, European Craton; CIB, Central Iran Blocks; GCB; Great Caucasian Basin; SCB, South Caspian Basin; LH, Lhasa Block; QI, Qiangtang Block; SG, Songpan-Garzê prism; Q, Qaidam Block; Mon, Mongolian Block; NC,

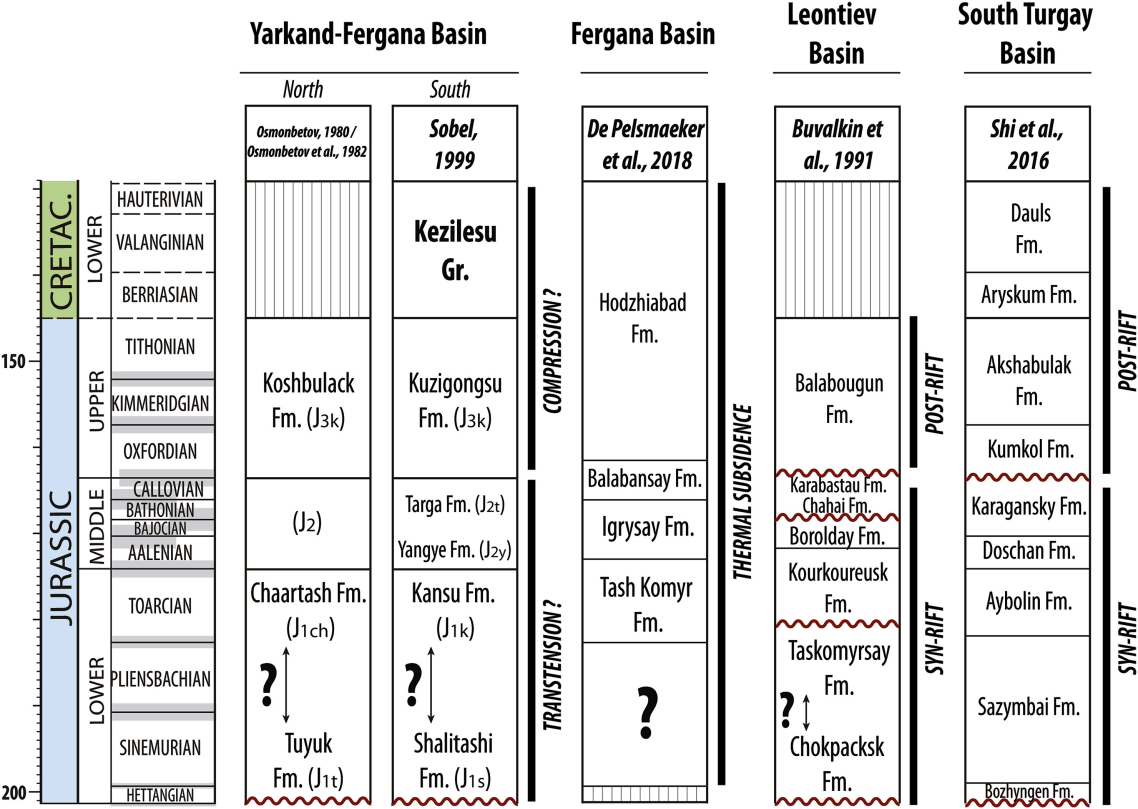
North China Block; SC, South China Block; IND, Indochina Block; SIB, Sibumasu Block; WB, West Burma Block; TFF, Talas Fergana fault. (B) Focus on the structural and kinematic pattern of the region extending from the Kyrgyz Tian Shan region to the Neo-Tethys subduction zone in present-day Iran (modified from Morin et al., 2018). ST: South Turgay Basin; LT: Leontiev Basin; YF: Yarkand Fergana Basin; TFF: Talas Fergana/Karatau fault; 1, Paleotethys suture; 2, Turkestan suture. The white arrows indicate the general direction of extension derived from the kinematic analysis of the major faults as reported by VNIGNI and Beicip Franlab (1992), Thomas et al. (1999), Robert et al. (2014), Brunet et al. (2017). The black arrows represent the inferred direction of slab-pull along the Neo Tethys subduction zone. The geometry of the latest is following Brunet et al. (2017).

Table 1 GPS coordinates of the analyzed sedimentary sections presented in this study.

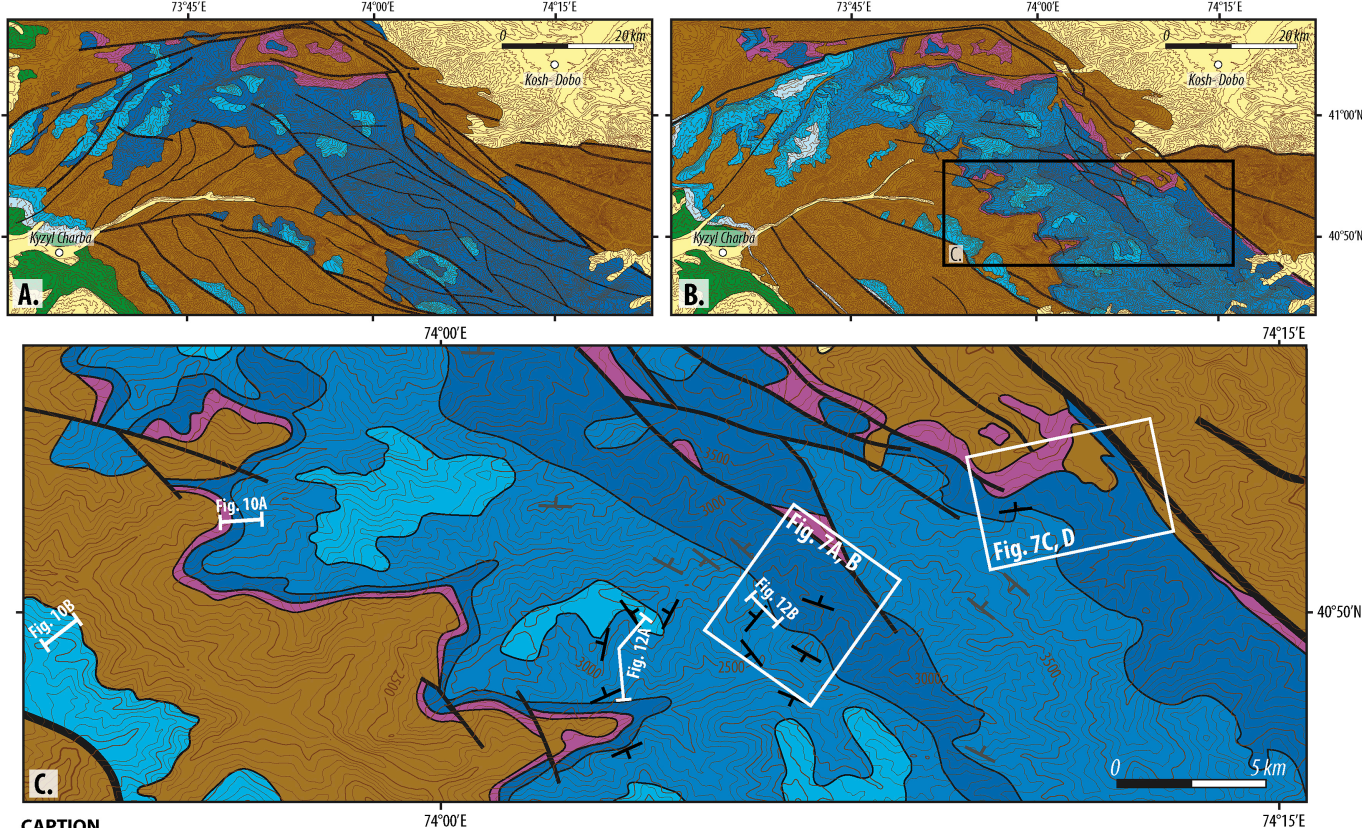
Table 2 Facies assemblage descriptions and their interpretations in terms of depositional environments.











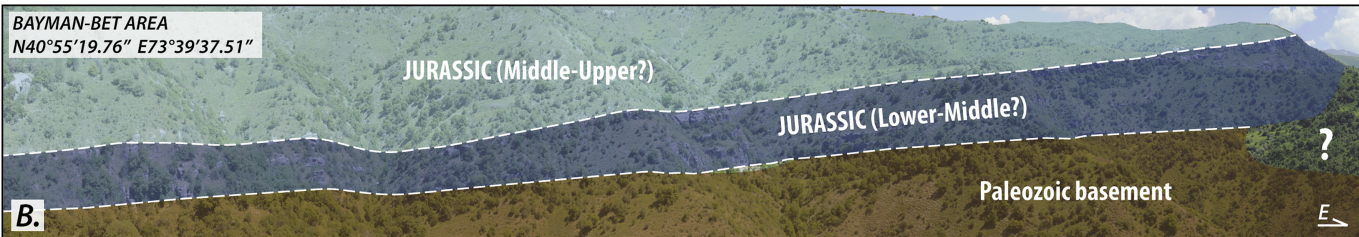
# CAPTION



BAYMAN-BET AREA  
N40°55'19.76" E73°39'37.51"

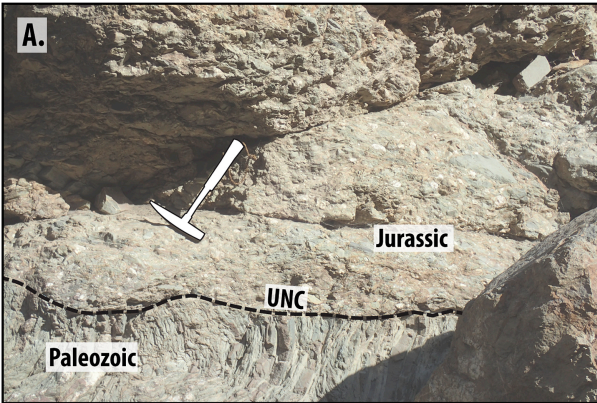


BAYMAN-BET AREA  
N40°55'19.76" E73°39'37.51"

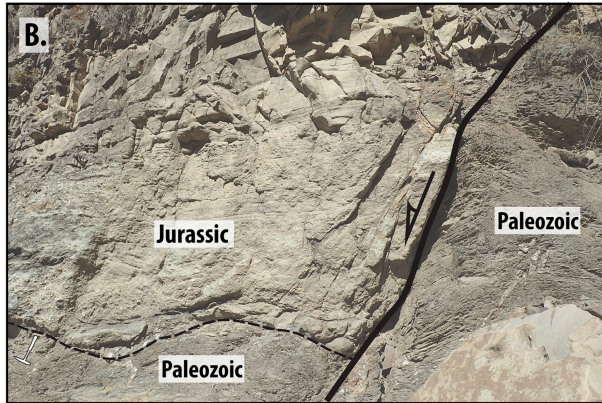




**A.**



**B.**



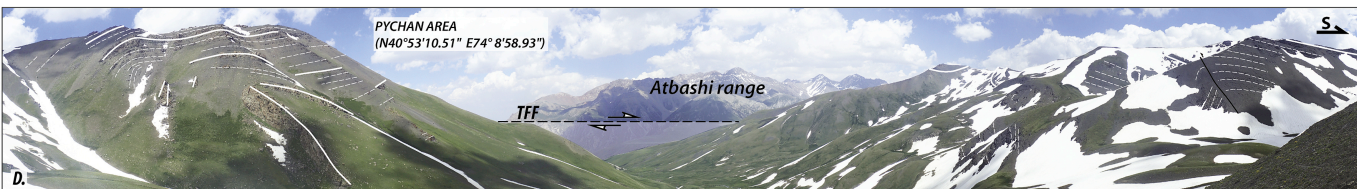
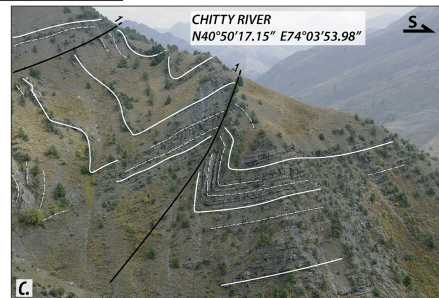


CHITTY RIVER  
N40°51'46.05" E74°07'19.81"

A.

CHITTY RIVER  
N40°51'03.50" E74°03'46.13"

B.



PYCHAN AREA  
(N40°53'10.51" E74°8'58.93")

E.

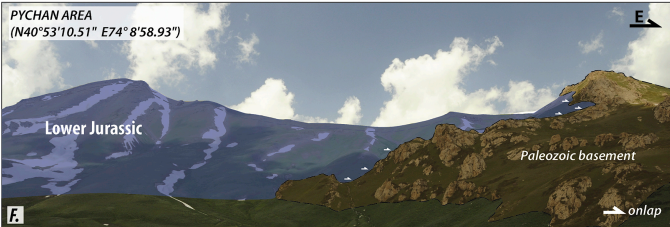
PYCHAN AREA  
(N40°53'10.51" E74°8'58.93")

F.

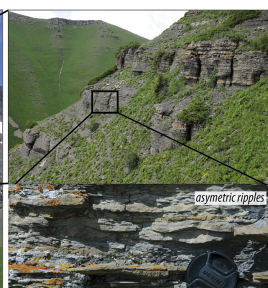
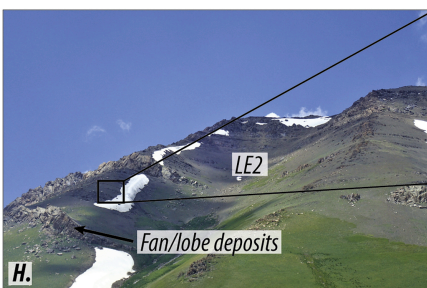
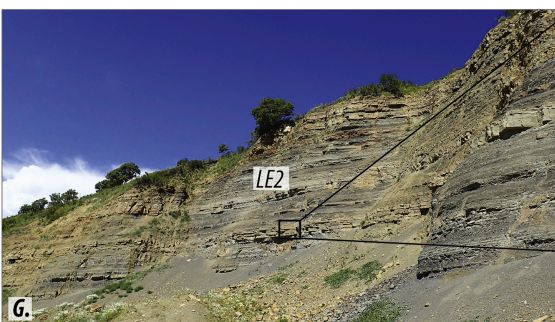
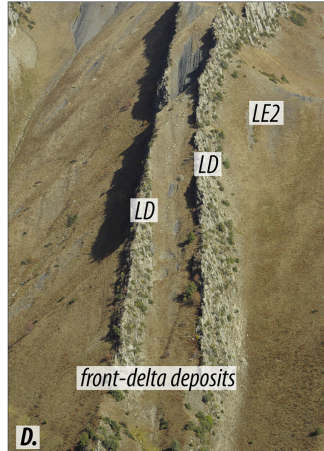
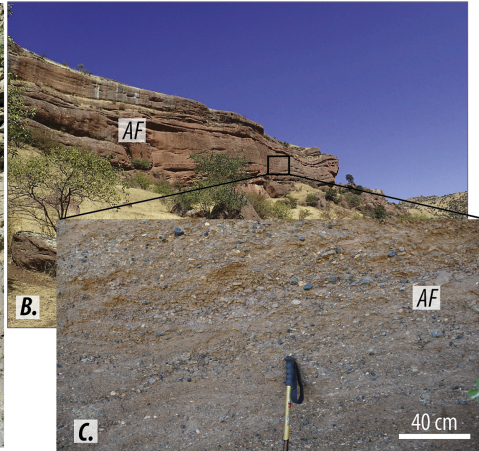
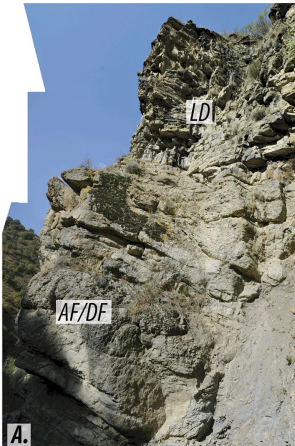
Lower Jurassic

Paleozoic basement

onlap

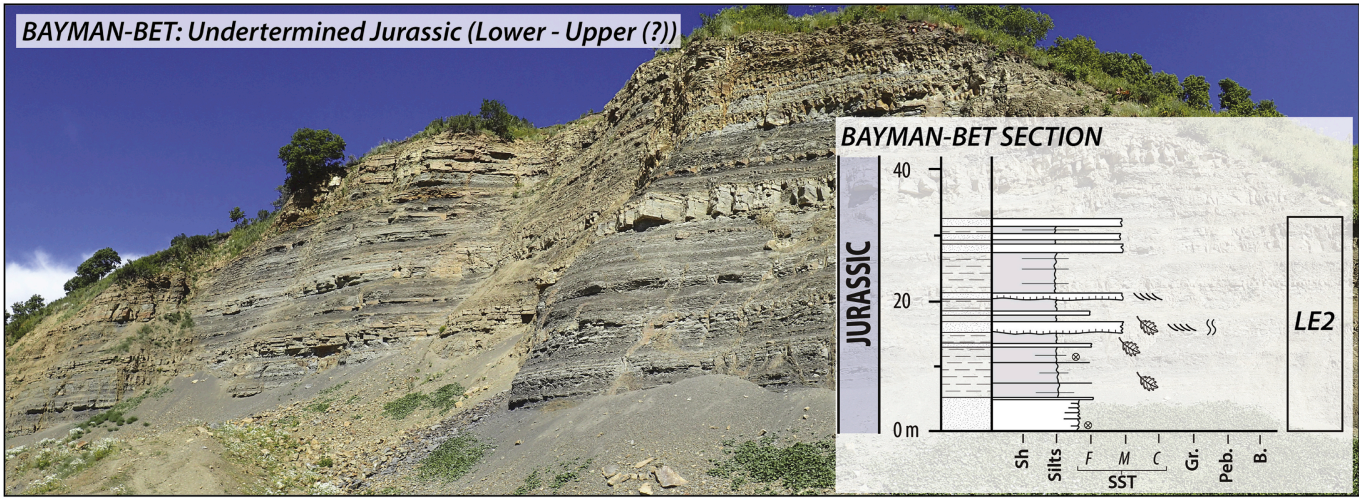






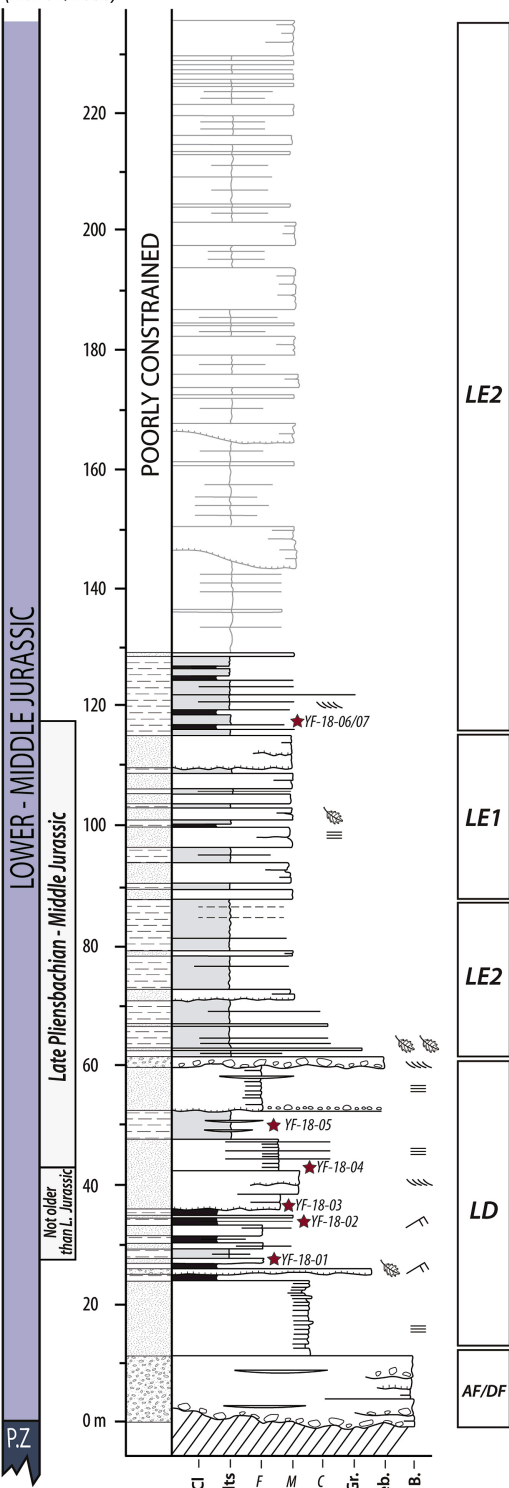


**BAYMAN-BET: Undertermined Jurassic (Lower - Upper ??)**



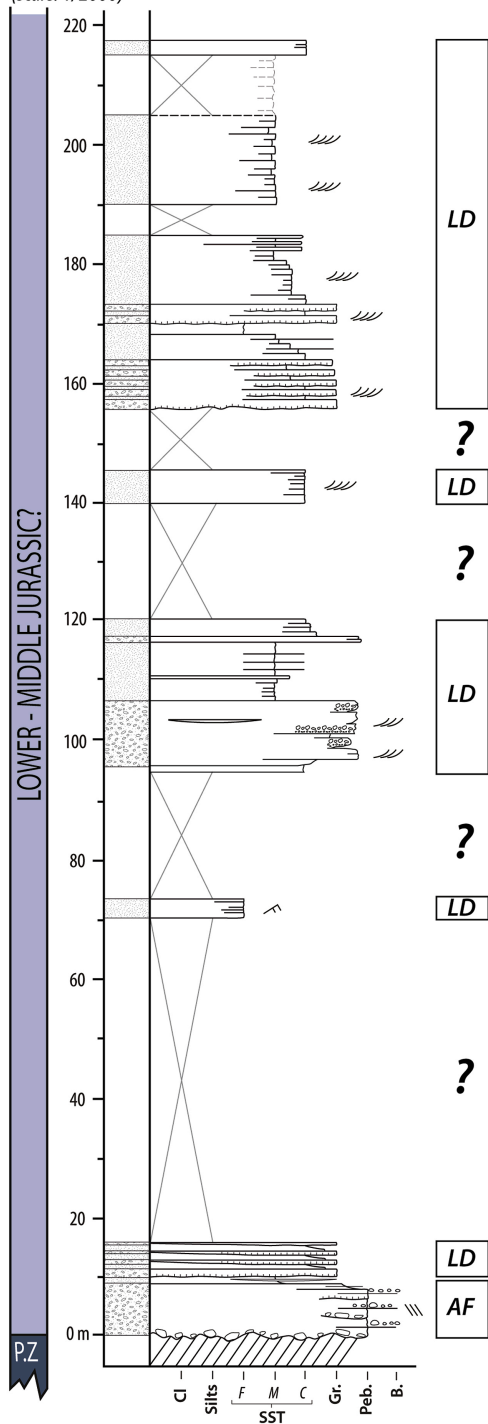
# A) KARA ALMA SECTION

(scale: 1/2000)



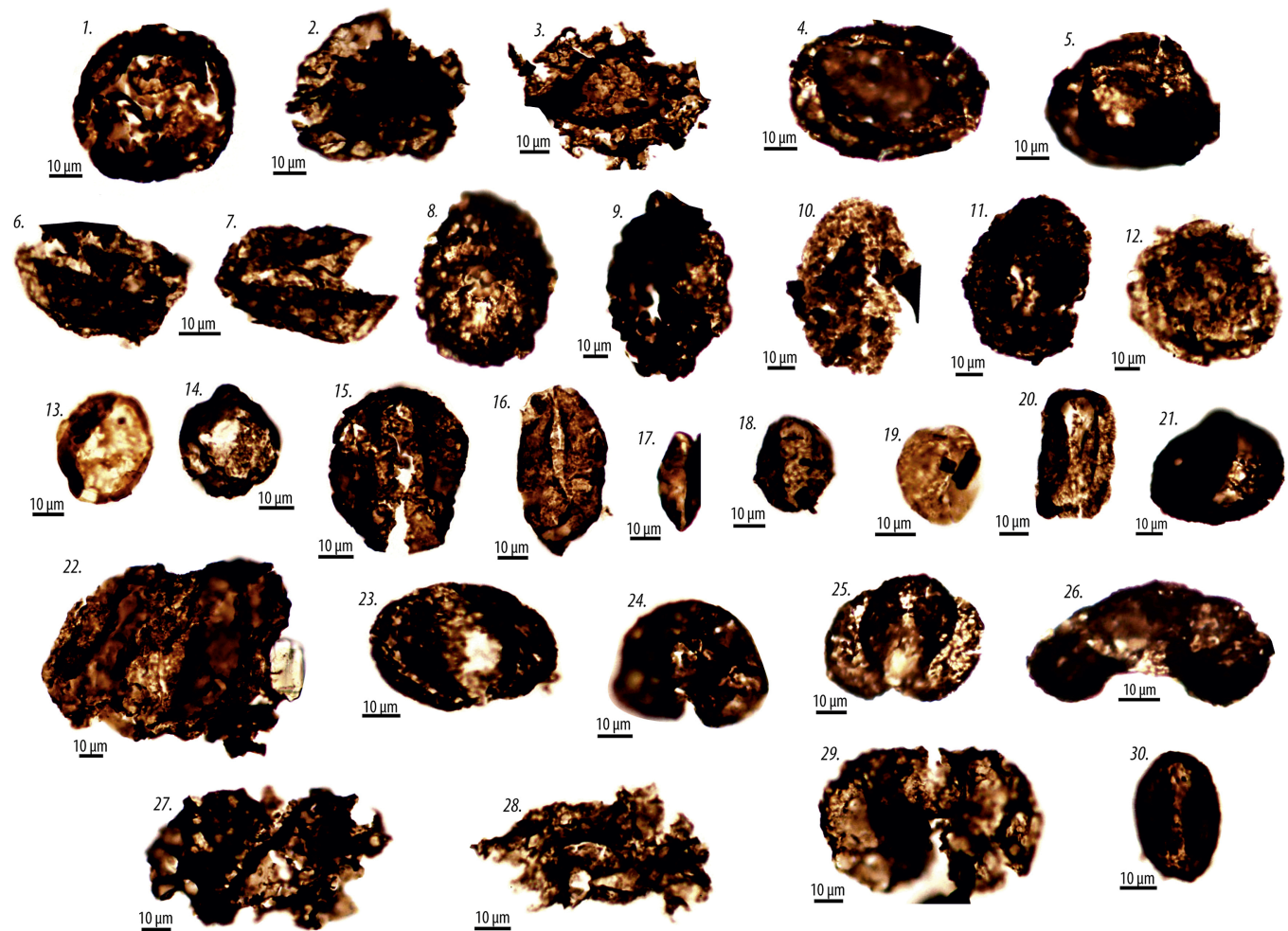
# B) KARA TUYBE SECTION

(scale: 1/2000)

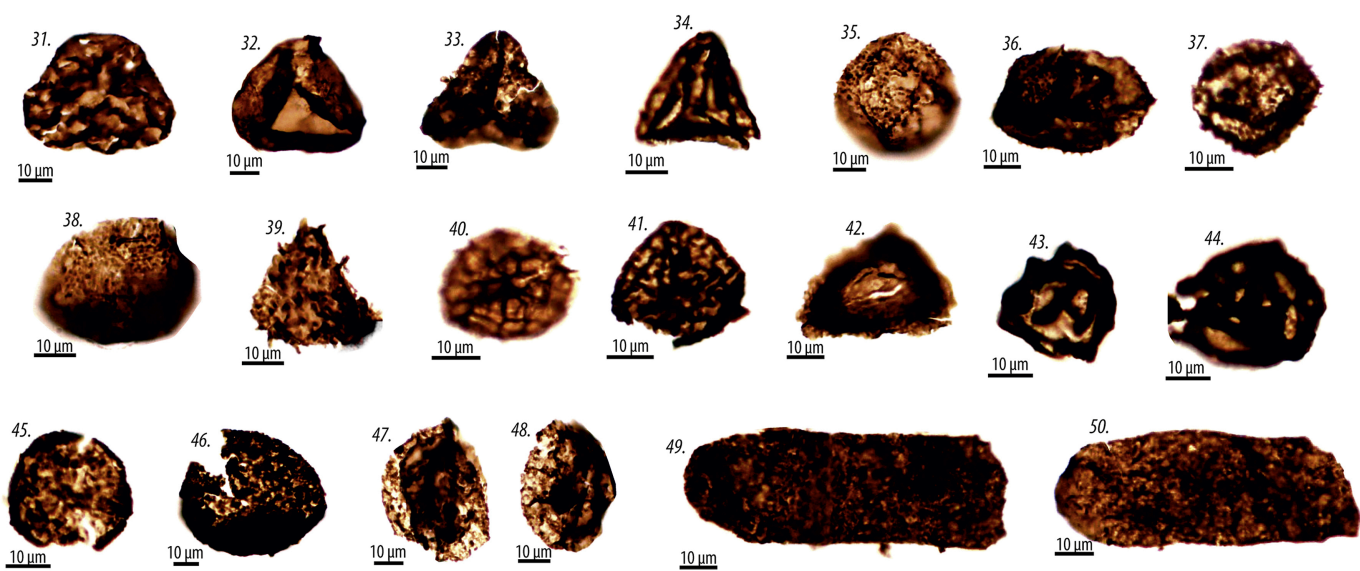


BEDDINGS	BIOTURBATIONS	SYMBOLS	LITHOLOGY	BASAL BOUNDARIES
Current ripples 2D megariipples 3D megariipples flat laminations Oscillatory ripples	Horizontal burrows Vertical burrows Pervasive Bioturbation	Plant fragments Root traces Rip-up clasts Normal grading Lenses or channels	Conglomerate Sandstone Coal-rich layer Siltstone Siltstone (grey/black)	Slightly erosional basal boundary Strongly erosional basal boundary <b>MISCELLANEOUS</b> Biostratigraphic sample

# POLLENS



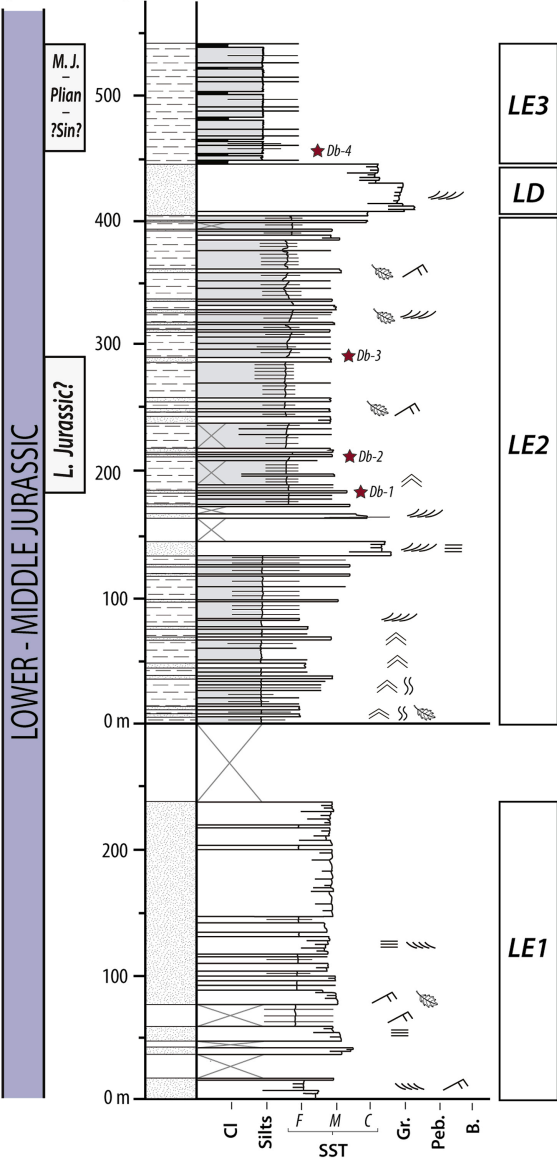
# SPORES





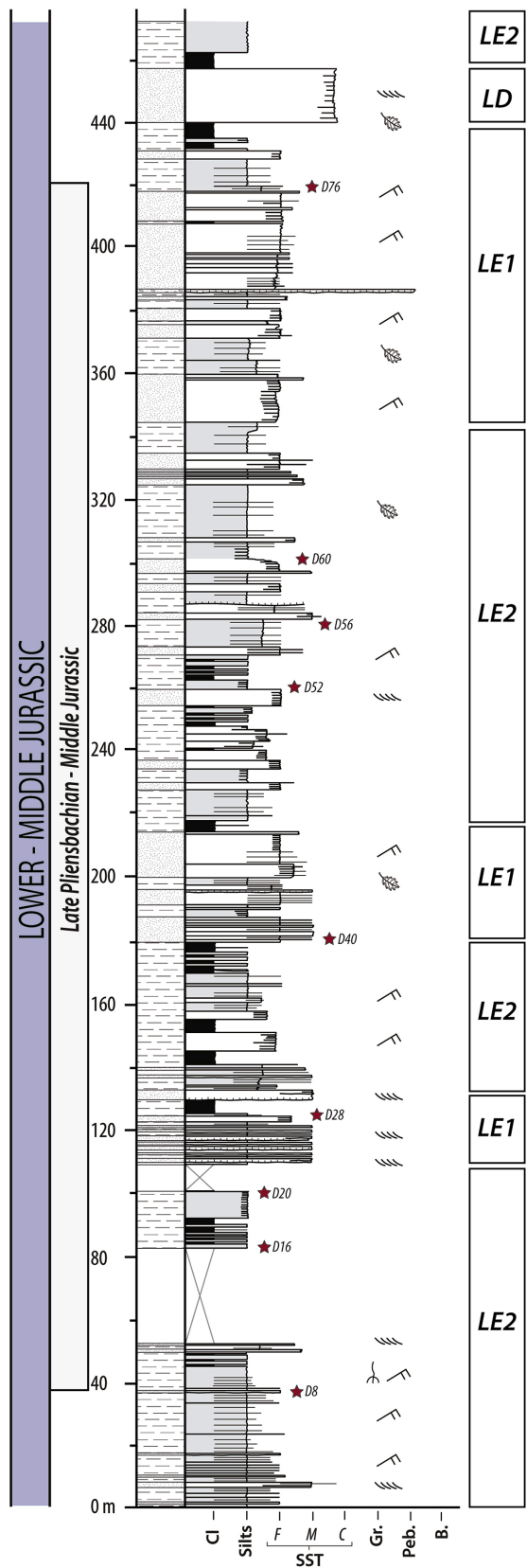
# A) WEST CHITTY SECTION

(scale: 1/5000)



# B) EAST CHITTY SECTION

(scale: 1/2000)



**PYCHAN SECTION: Lower Jurassic**

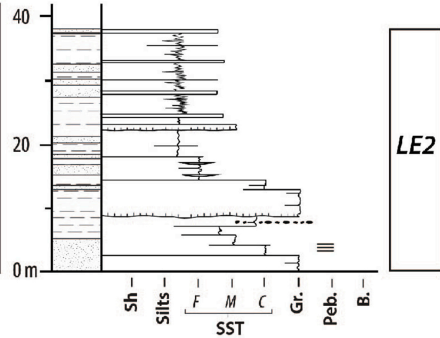
**E** ↗



**Fan/lobe systems**

**PYCHAN SECTION**

**LOWER JURASSIC?**



**A.**



*Lower Jurassic*

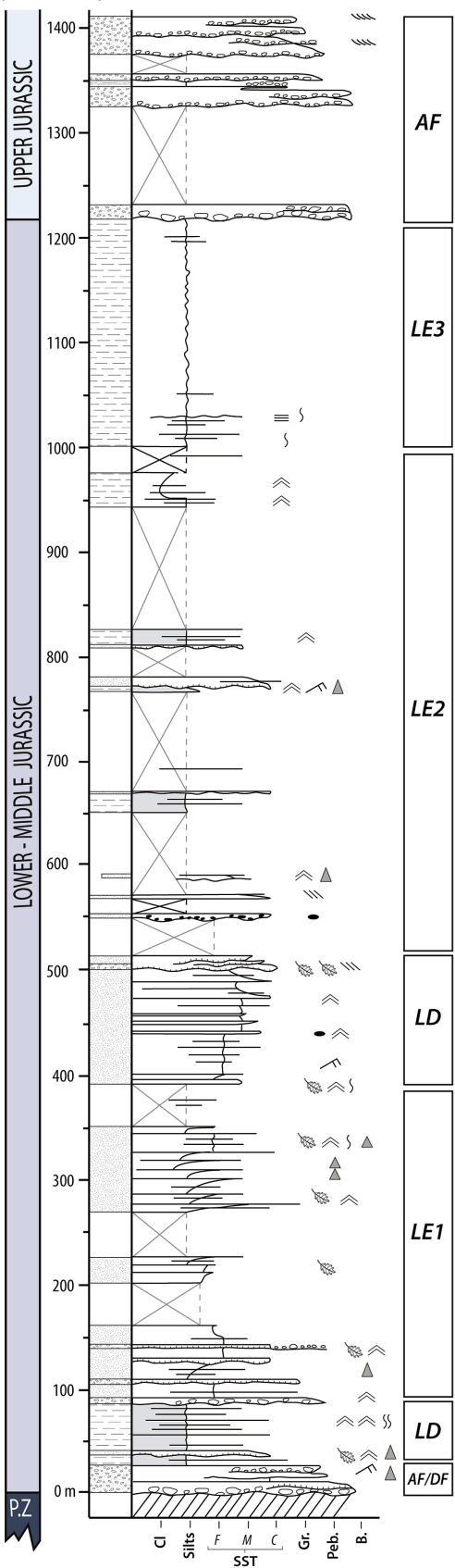
*Paleozoic basement*

*onlap*

**B.**

# TEREK SECTION

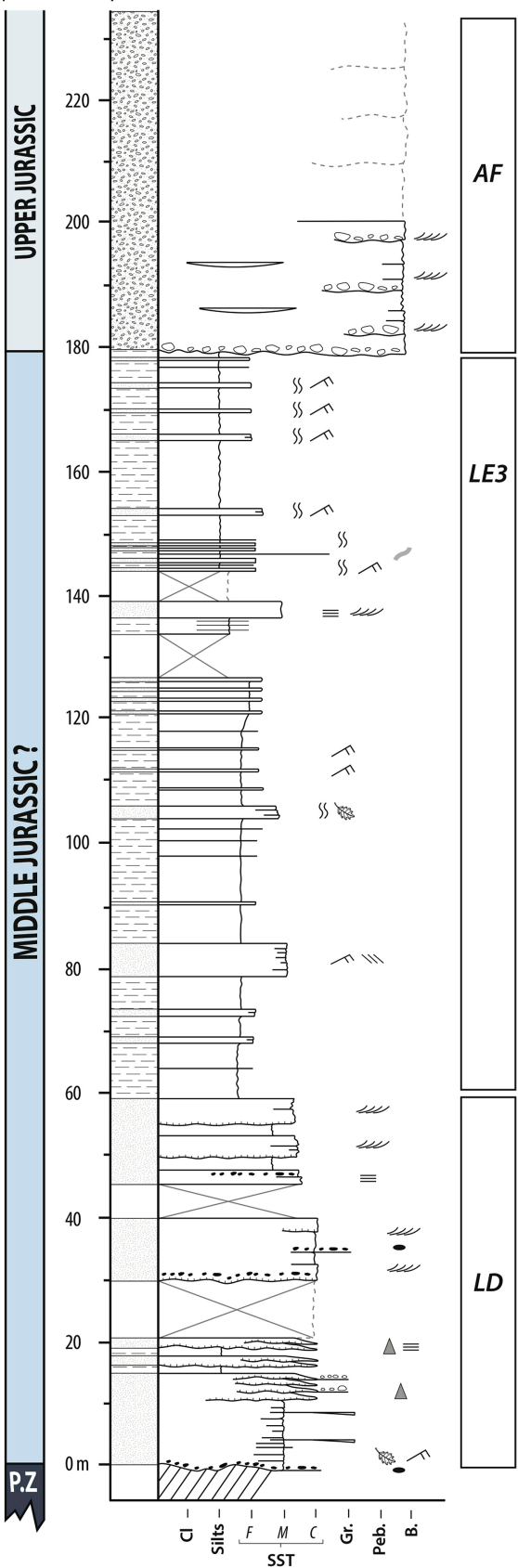
(scale: 1/5000)



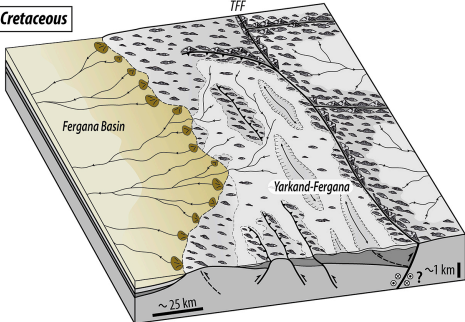


# YASSY RIVER SECTION

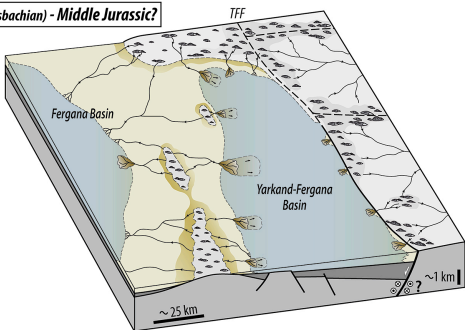
(scale: 1/2000)



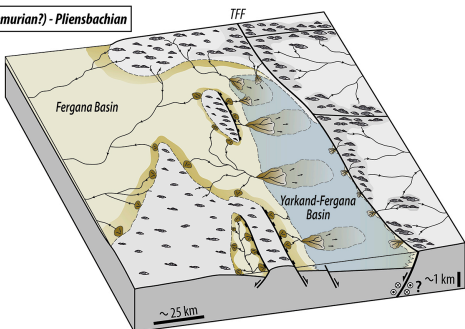
#### D) Late Jurassic - Early Cretaceous



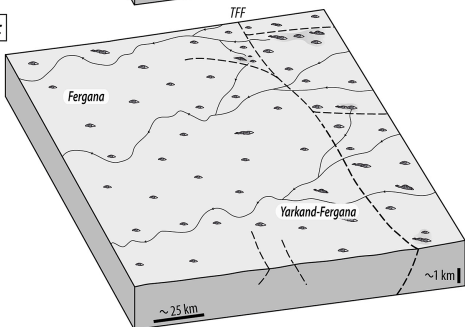
#### C) Late Early (Late Pliensbachian) - Middle Jurassic?



#### B) Early Jurassic: (Sinemurian?) - Pliensbachian



#### A) Middle-Late Triassic



#### PALEOGEOGRAPHY

Proximal alluvial plain	Low relief
Distal alluvial plain	Medium-low relief
Lake	Hills
Alluvial fans	Mountains
Deltas	Potential drainage direction

#### SEDIMENTARY SERIES

Late Early (Late Pliensbachian) - Middle Jurassic
Early Jurassic: Sinemurian? - Pliensbachian

#### TECTONICS

Active fault
Relatively Inactive fault
Fold

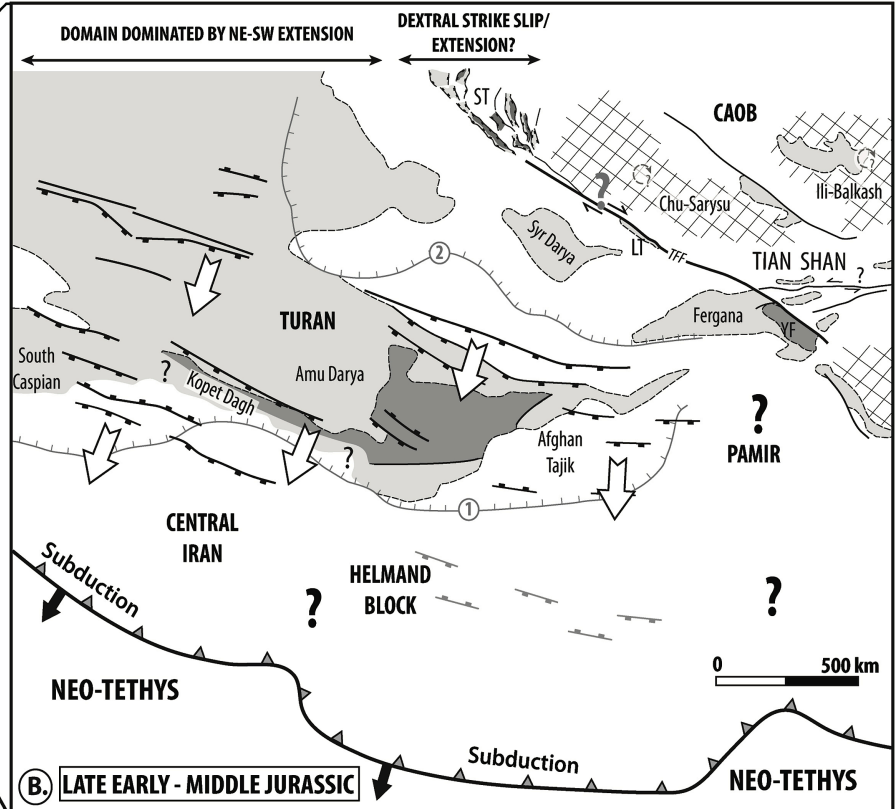
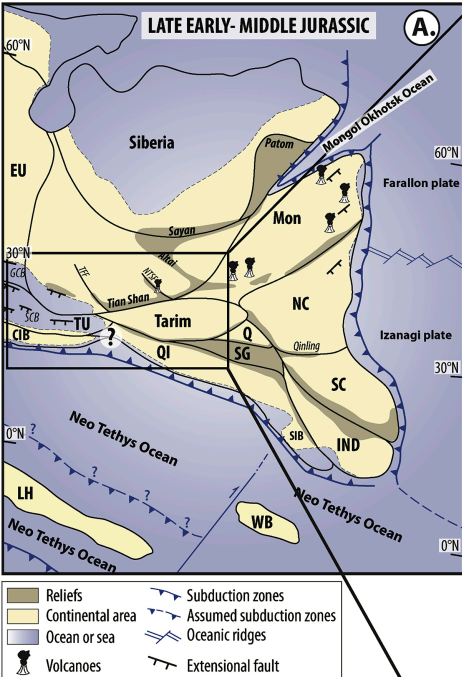


Table 1 GPS coordinates of the analyzed sedimentary sections presented in this study.

<b>Sedimentary sections</b>	<b>Latitude (N)</b>	<b>Longitude (E)</b>
Bayman-Bet	40°55'19.76"	73°39'37.51"
Kara Alma	40°53'13.70"	73°56'15.50"
Kara Tuybe	40°51'5.60"	73°53'19.30"
West Chitty	40°50'12.90"	74° 3'41.30"
East Chitty	40°51'13.11"	74° 5'46.83"
Pychan	40°53'10.51"	74° 8'58.93"
Yassy	40°49'55.05"	73°36'47.16"
Terek	40°24'0.78"	74°21'53.58"

<i><b>Facies assemblages</b></i>	<i><b>Main sedimentary features</b></i>	<i><b>Inferred depositional environment</b></i>
<b>AF/DF</b> (Fig. 8A, B, C)	<p>Alternation of:</p> <ul style="list-style-type: none"> <li>- Pluri dm- to pluri m- thick clast-supported conglomerate of poorly to moderately-sorted subangular to subrounded pebbles to boulders alternating with cm to m-thick medium to coarse grained sandstones containing floating gravels. Conglomerates are massive with erosive or sharp basal boundaries and occasional pebble imbrications. Sandstone beds are tabular or lenticular and can be structureless or contain planar laminations and trough cross bedding with</li> <li>- m- to pluri m-thick matrix-supported conglomerate with subangular to subrounded pebbles to boulders, poorly-sorted. Conglomerates are generally massive and present sometimes faint horizontal laminations.</li> </ul>	<b>Alluvial fan or Delta fan environments</b> characterized by hyperconcentrated flows, streamflow and debris flow deposits (Miall, 1978; Postma, 1990; Miall 1996; Svendsen et al., 2003).
<b>LD</b> (Fig. 8D, E)	<ul style="list-style-type: none"> <li>- m- to several m-thick heterolithic facies with dm- to m-thick fine-grained sandstone beds showing current and oscillatory ripples, alternating with dm- to m-thick siltstone beds, locally organic-rich. This heterolithic facies is interbedded with m-thick coarse-grained to pebbly sandstone showing occasional erosive basal boundaries, inverse and normal grading, and vertical burrows.</li> <li>- dm- to pluri-m- thick stacked medium grained to gravelly sandstone beds containing flat-laminations, trough and planar cross-stratification, sigmoidal beddings.</li> </ul>	<b>Lacustrine delta environment</b> characterized by <b>mouth bars and front delta deposits</b> (Postma, 1990; Marshall, 2000; Bhattacharya, 2010).
<b>LE1</b> (Fig. 8F)	<p>m- to several m-thick heterolithic facies composed of an alternation of:</p> <ul style="list-style-type: none"> <li>- one dm to pluri-m-thick fine to coarse-grained sandstone with sharp, sometimes erosional basal boundaries showing current and oscillatory ripples, numerous plant fragments, occasional inverse and normal grading and bioturbations alternating with</li> <li>- one cm to m-thick organic-rich siltstone with occasional coal beds.</li> </ul>	<b>Lacustrine environment dominated by turbiditic sand deposits</b> (Pollard et al., 1982; Hinds et al., 2004; Bhattacharya, 2010).

<b>LE2</b> (Fig. 8G, H)	cm- to m- thick homolithic organic-rich siltstones with occasional coal beds alternating with pluri cm- to m- thick fine to medium grained sandstone beds with sharp basal boundaries showing current and rare wave ripples, occasional grading and bioturbation. Occasional m- to pluri-m-thick sandstone beds with sharp basal boundaries and generally presenting convex-up geometries. These beds are generally graded from gravels to fine-grained sandstone and show flat-laminations.	<b>Lacustrine environment</b> dominated by <b>suspension fallout and fan/lobe systems</b> (Pollard et al., 1982; Reynolds et al., 1998).
<b>LE3</b> (Fig. 8J, I)	Massive, horizontally laminated siltstones with cm to m-thick fine to medium grained sandstone beds. Occasional bioturbation	<b>Distal lacustrine environment</b> dominated by <b>suspension fallout and biological activity</b> (Pollard et al., 1982; Reynolds et al., 1998).

Table 2: Facies assemblage descriptions and their interpretations in terms of depositional environments.

First sedimentology and palynology data from the Jurassic Yarkand-Fergana Basin

Sinemurian(?) – Pliensbachian onset of sedimentation in half graben setting

Extension led to Middle Jurassic basin widening before Early Cretaceous inversion

Jurassic movements along the Talas Fergana Fault is not associated to Qiangtang collision

**Declaration of interests**

The authors declare that they have no known competing financial interests or personal relationships that could have appeared to influence the work reported in this paper.